photonics

MDPI

Review

Review of Artifacts and Related Processing in Ophthalmic Optical Coherence Tomography Angiography (OCTA)

Zhefan Lin [1,†], Yitao Hu [1,†], Gongpu Lan [1,2], Jingjiang Xu [1,2], Jia Qin [2], Lin An [2] and Yanping Huang [1,2,*]

[1] Guangdong-Hong Kong-Macao Joint Laboratory for Intelligent Micro-Nano Optoelectronic Technology, School of Physics and Optoelectronic Engineering, Foshan University, Foshan 528000, China; 2112155012@stu.fosu.edu.cn (Z.L.); 2112205017@stu.fosu.edu.cn (Y.H.); langongpu@fosu.edu.cn (G.L.); jaysonxu25@gmail.com (J.X.)

[2] Innovation and Entrepreneurship Teams Project of Guangdong Provincial Pearl River Talents Program, Guangdong Weiren Meditech Co., Ltd., Foshan 528015, China; wrqinjia@weirenmeditech.com (J.Q.); wranlin@weirenmeditech.com (L.A.)

* Correspondence: yale.huangyp@fosu.edu.cn; Tel.: +86-13660026462

† These authors contributed equally to this work.

Abstract: Optical coherence tomography angiography (OCTA) is a non-invasive imaging modality that can provide rich three-dimensional microvascular information of fundus in ophthalmic imaging. However, various imaging artifacts may be generated during OCTA data acquisition and processing, originating from a number of factors such as multiple light scattering, tissue motion, improper device operation and signal processing algorithms. Artifacts can detrimentally affect the qualitative interpretation of clinical pathologies and quantitative evaluation of vasculature parameters. This article firstly introduces the OCTA acquisition process and sources of artifacts, and then describes four different categories of artifacts in detail, mainly including light propagation and signal intensity-related artifacts, tissue motion artifacts, improper operation artifacts, and signal processing-related artifacts. Corresponding methods for the identification and processing of these artifacts are also presented. Furthermore, this article also details some recent progress in leveraging artificial intelligence (AI) technology in the identification and suppression of artifacts, showcasing its potential as a powerful tool in OCTA artifact processing. The development of artifact suppression techniques enables OCTA to reliably evaluate fundus diseases and monitor their progression. This development facilitates broader and deeper applications of OCTA in both research and clinics of ophthalmology.

Keywords: optical coherence tomography angiography; image artifact; artifact processing; projection artifact; motion artifact

check for updates

Received: 8 April 2025
Revised: 20 May 2025
Accepted: 22 May 2025
Published: 25 May 2025

Citation: Lin, Z.; Hu, Y.; Lan, G.; Xu, J.; Qin, J.; An, L.; Huang, Y. Review of Artifacts and Related Processing in Ophthalmic Optical Coherence Tomography Angiography (OCTA). *Photonics* **2025**, *12*, 536. https://doi.org/10.3390/photonics12060536

Copyright: © 2025 by the authors. Licensee MDPI, Basel, Switzerland. This article is an open access article distributed under the terms and conditions of the Creative Commons Attribution (CC BY) license (https://creativecommons.org/licenses/by/4.0/).

1. Introduction

Optical coherence tomography (OCT) is a noninvasive imaging technology based on low-coherence interferometry, capable of generating cross-sectional images of biological tissues with micrometer-scale resolution [1]. By detecting backscattered light from tissue microstructures, OCT enables rapid, real-time visualization of tissue layers and fine anatomical features without requiring exogenous contrast agents [2]. Modern OCT systems integrate high-speed scanning with exceptional spatial resolution, establishing this technology as an indispensable tool in both research and clinical practice [3]. Building upon OCT's technological strengths, optical coherence tomography angiography (OCTA) extends its utility to high-resolution three-dimensional (3D) images of tissue microvascular

networks [4,5]. The basic principle of OCTA is to detect the contrast caused by the motion of substances, mainly red blood cells in the vessels, and thus display the contrast of microvasculature versus static tissues [6,7]. The OCTA imaging process mainly involves repeated B-scan imaging at the same location, and then calculating the changes in phase [8,9], amplitude [10,11], or complex signal [12–14] over time as the contrast mechanism.

To visualize vascular changes in the fundus, common angiography techniques in clinical practice are fluorescein fundus angiography (FFA) and indocyanine green angiography (ICGA). The former typically displays the retinal vascular system, while the latter is used for imaging the choroidal vascular system due to their different capabilities in imaging depths [4,15]. However, both methods are invasive with the need for dye injection and a period of 10–15 min for taking images [5]. Moreover, they may cause side effects: the dye may trigger serious adverse reactions, such as gastrointestinal side effects or anaphylactic shock, and patients who are pregnant or have liver or kidney impairment cannot take these tests [16,17]. OCTA can obtain images quickly in a non-invasive and dye-free way, avoiding dye-related side effects. In addition, FFA and ICGA only provide two-dimensional images without depth-related information. OCTA can produce high-resolution cross-sectional images at the micron level and reveal the three-dimensional structure of the microvascular network. It can also segment different layers along the depth direction, enabling the display of clinically useful en-face OCTA images at various depths.

Due to these advantages, OCTA is a widely used technique for ophthalmic imaging and studying various eye diseases, especially vascular diseases, such as age-related macular degeneration (AMD), diabetic retinopathy (DR), retinal vein occlusion (RVO), and choroidal neovascularization (CNV) [18]. As technique advances, OCTA has evolved from qualitative to quantitative analysis. Researchers have shown that quantitative measurements on OCTA images, such as vascular density and foveal avascular zone (FAZ), can differentiate normal healthy eyes from pathological eyes [19–21], providing objective evidence for disease diagnosis.

However, OCTA is an emerging technology that still has some limitations in its applications. It cannot detect vascular leakage or slow blood flow below its detection threshold [22], and it is challenging to measure blood flow velocity in a quantitative way. Single OCTA scanning field of view is generally smaller than other angiographic imaging techniques [23]. A major limitation of OCTA is the presence of artifacts, which are incorrect or misleading structures observed in the images that do not reflect the true condition of the scanned tissue. Artifacts affect the presence of OCTA data and image assessment and even may lead to false conclusions [24]. Various sources can cause artifacts, such as data acquisition, image processing, OCTA system properties, or tissue structure abnormalities.

The presence of artifacts in OCTA affects the ability of this technology to obtain accurate vascular network images in clinical settings and consequently reduces the accuracy of quantitative vascular parameters. Studying the artifacts and their processing methods in OCTA can help better describe the spatial morphology, distribution, and changes in the vascular network, which is of great significance for the diagnosis and evaluation of vascular diseases. This article reviews the current status of artifact research in OCTA, starting from the acquisition process and the sources of artifacts in OCTA, and introduces various types of artifacts and their elimination or suppression methods in detail. It further explores approaches for leveraging artificial intelligence technology in OCTA artifact processes. Finally, it concludes by presenting the latest advancements and future research directions in related topics.

2. OCTA Data Acquisition Process and Artifact Generation

Optical coherence tomography (OCT) systems use the basic principle of low-coherence light interference to obtain the light scattering information of the sample along the depth by using various hardware components, which typically include a broadband near-infrared light source, Michelson interferometer, and spectrometer in spectral domain OCT. OCT angiography is a functional extension of OCT imaging which is used for the extraction of tissue vascular information. The quality of OCTA imaging highly depends on various factors including the OCT hardware system, the scanning mode, and the blood flow signal generation algorithm. The common scanning mode for OCTA involves multiple repeated B-scans at the same location and comparing the repeatedly scanned images pixel by pixel to detect the motion contrast of flowing red blood cells relative to stationary tissue. The detected motion signal is then used as a contrast mechanism to generate an OCTA image.

An OCT signal is inherently a complex-valued function comprising both amplitude and phase components, which can be expressed as:

$$C_{OCT}(x,\ z,\ t) = I(x,\ z,\ t)e^{-i\Phi(x,\ z,\ t)} \tag{1}$$

where $I(x,\ z,\ t)$ represents the amplitude and $\Phi(x,\ z,\ t)$ denotes the phase at the lateral position x, the depth position z, and the time t. Depending on the components used to extract blood flow information, OCTA methodologies can be broadly classified into three categories: phase-signal-based, intensity-signal-based, and complex-signal-based approaches. A representative phase-signal-based method is phase variance OCTA [8,9]. In this method, the flow signal, which is computed from a series of consecutive B-scans at the same location, can be expressed as follows:

$$Flow_{PV}(x,\ z) = \frac{1}{N-1}\sum_{j=1}^{N-1}\left[\Delta\Phi_j(x,\ z) - \frac{1}{N-1}\sum_{i=1}^{N-1}\Delta\Phi_i(x,\ z)\right]^2 \tag{2}$$

$$\Delta\Phi_i(x,\ z) = \Delta\Phi_i(x,\ z,\ t) = \Phi_{i+1}(x,\ z,\ t+T) - \Phi_i(x,\ z,\ t) \tag{3}$$

where N represents the number of repeated B-scans acquired at the same location; $\Phi_i(x,\ z)$ and $\Delta\Phi_i(x,\ z)$ represent the phase value and phase difference in the i-th B-scan at the lateral position x, the depth z, and the time t; T is the time interval between two consecutive B-scans; and i (or j) is the index of the i-th (or j-th) B-scan. Two commonly used intensity-signal-based OCTA methods are speckle variance OCTA [10,25] and split-spectrum amplitude-decorrelation angiography (SSADA) [26]. The speckle variance OCTA is given by:

$$Flow_{SV}(x,\ z) = \frac{1}{N}\sum_{i=1}^{N}(I_i(x,\ z) - I_{mean})^2 \tag{4}$$

$$I_{mean} = \frac{1}{N}\sum_{i=1}^{N} I_i(x,\ z) \tag{5}$$

where N represents the number of B-scans repetitions at the same location, $I_i(x,\ z)$ denotes the intensity value at the lateral position x and the depth z in the i-th B-scan, and I_{mean} is the average of the intensity value over the same set of pixels. The SSADA algorithm is expressed as:

$$Flow_{SSADA}(x,\ z) = 1 - \frac{1}{N-1}\frac{1}{M}\sum_{i=1}^{N-1}\sum_{m=1}^{M}\frac{I_{im}(x,z)I_{(i+1)m}(x,z)}{\left[\frac{1}{2}I_{\mathrm{im}}(x,z)^2 + \frac{1}{2}I_{(i+1)m}(x,z)^2\right]} \tag{6}$$

where M is the number of split spectrums, N is the number of repeated B-scans, and $I_{im}(x,z)$ represents the intensity value at the position (x, z) in the i-th B-scan of the m-th split spectrum. The representative of the complex-signal-based OCTA technique is optical microangiography (OMAG) [12]. The flow signal based on the OMAG algorithm is calculated by subtracting consecutive complex signals, as shown in the following equation:

$$Flow_{OMAG}(x,\ z) = \frac{1}{N-1}\sum_{i=1}^{N-1}|C_{i+1}(x,\ z) - C_i(x,\ z)| \tag{7}$$

where N is the number of repeated B-scans at the same location, and $C_i(x,\ z)$ represents the complex OCT signal, comprising both intensity and phase components at the lateral position x and depth z in the i-th B-scan.

OCTA images may display vascular information that is different from its true situation. This is called an OCTA image artifact, which is a visual defect or abnormality shown in the image caused by various factors. Artifacts can occur at any step of the imaging process and may be related to the subject, operator, or system. To some extent, artifacts related to the patient and operator can be avoided by proper and accurate operation, while artifacts related to signal processing are caused by the processing algorithm, and advanced processing methods are needed to suppress these artifacts [27]. Figure 1 illustrates the main steps and objects involved in the OCTA imaging process and the types of artifacts that may arise from tissue defects or imaging limitations. Based on the imaging steps involved or their characteristics, artifacts are divided into the following four categories in this study, which are specifically described in the subsequent section.

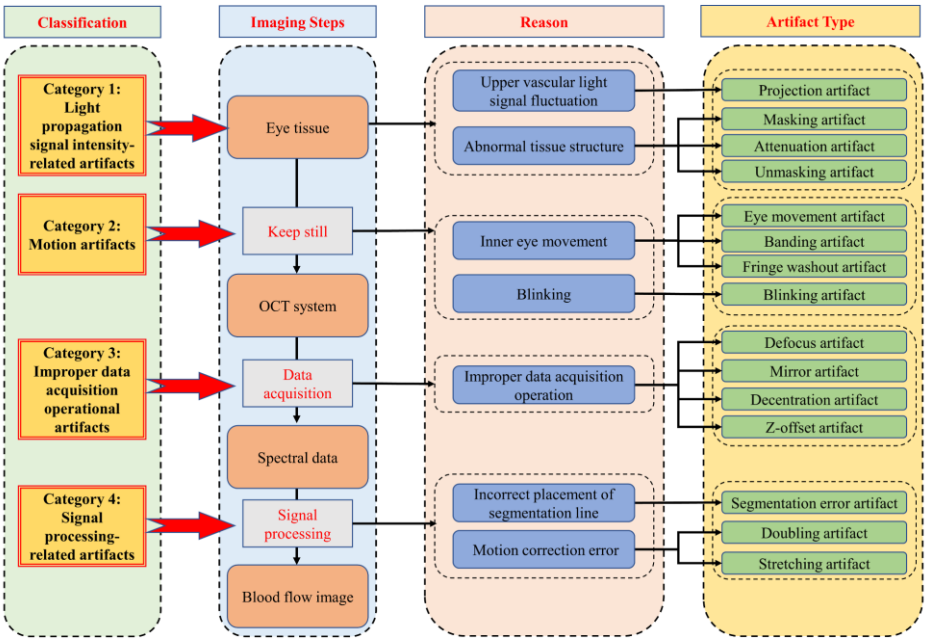


Figure 1. Main processes involved in OCTA imaging and related artifact types.

The first category of artifacts are light propagation and signal intensity-related artifacts. The optical signal of the deep tissue will be affected by the fluctuation of the shallow vascular tissue signal in light propagation, which will cause one of the most important OCTA artifacts, the projection artifact. Too large or small signal intensity will cause OCTA artifacts including masking artifacts, attenuation artifacts, and unmasking artifacts.

The second category of artifacts are motion artifacts. High-quality eye OCTA data acquisition requires the subject to be stationary. Involuntary eye movement, respiratory movement, and pulse beating during data acquisition cause eye movement artifacts, band-

ing artifacts, and fringe washout artifacts. In addition, blinking during the acquisition process causes partial signal loss in the OCTA image, which is called a blinking artifact.

The third category of artifacts is caused by improper operation or suboptimal imaging conditions during the acquisition process, resulting in defocus artifacts, mirror artifacts, decentration artifacts, and Z-offset artifacts.

The fourth category of artifacts is caused by incorrect signal processing during the vascular image generation process, mainly including segmentation error artifacts. Moreover, image processing steps such as motion correction may also generate new artifacts, such as doubling artifacts and stretching artifacts.

3. Types and Processing of Artifacts

Artifacts are one of the main factors that affect the quality of OCTA images. Figure 1 shows the different categories and causes of OCTA artifacts. This article describes in detail the definition, image presentation, and processing methods to eliminate these common artifacts reported in the literature. Table 1 summarizes the main types and their simple descriptions of OCTA artifacts. Identifying these artifacts can help accurately interpret OCTA images in clinical settings, which can guide the diagnosis and management of different retinal diseases. It should be noted that this article does not cover all types of OCTA artifacts. Some artifacts are not mentioned in this article, such as the hyper-reflective artifact caused by hyper-reflection signals in amplitude-base OCTA algorithms, as described by Huang et al. [28]. Interested readers can refer to the specific literature for their detailed illustration.

Table 1. Types and simple descriptions of various artifacts in OCTA images.

Artifact Category	Artifact Type	Artifact Description
Light propagation and signal intensity-related artifacts	Projection artifact	Blood flow tail phenomenon in depth inherently caused by mechanism of optical propagation
	Masking artifact	Blood flow shadowing below light-blocked area
	Attenuation artifact	Loss of real blood flow or emergence of noise-induced false blood flow caused by thresholding of weak OCT signal
	Unmasking artifact	Abruptly enhanced blood flow caused by strong incident optical intensity resulting from degradation of superficial tissues
Motion artifacts	Eye movement artifact	Horizontal or vertical white lines caused by transient eye movement
	Banding artifact	Abnormal wide stripes arising from eye movement lasting for a certain long period
	Fringe washout artifact	Dark choroidal large vessels caused by interference fringe washout effect
	Blinking artifact	Vertical or horizontal dark line in image due to subject blinking
Improper operation artifacts	Defocus artifact	Loss of small vessels caused by light defocusing of scan region
	Mirror artifact	Image folding around the zero-delay reference line leading to inverted tissues in part of the image
	Decentration artifact	Fovea is off-center in planned fovea-centered scanning
	Z-offset artifact	Abnormal image area created by a portion of the scanned tissue vertically shifted beyond the imaging area
Signal processing-related artifacts	Segmentation error artifact	Partial incorrect layer segmentation leading to false blood flow information
	Doubling artifact	Doubling of the same vessel caused by improper processing of eye movement correction
	Stretching artifact	Short stripes with varying brightness at the edge of OCTA images caused by incorrect vessel registration

3.1. Light Propagation and Signal Intensity-Related Artifacts

3.1.1. Projection Artifact

OCT is a depth imaging technique that utilizes the backscattering of light from tissues at different depths. Based on the propagation principle, the OCT signal from deeper tissues is inevitably influenced by the transmission of light from the preceding tissues. Projection artifacts refer to the fluctuating signal in the depth direction transmitted by the red blood cells in the superficial vasculature, which causes the OCT signal reflected by the underlying tissue to change with time, creating an illusion of blood flow tissue in its depth and resulting in a vascular artifact in the depth direction [18,29]. In the B-scan cross-sectional angiography image, the projection artifact is manifested as an axial extension of blood flow signal like a tail, thus also being called the "tail artifact" [30]. Figure 2 shows the typical projection artifacts in OCTA images [31].

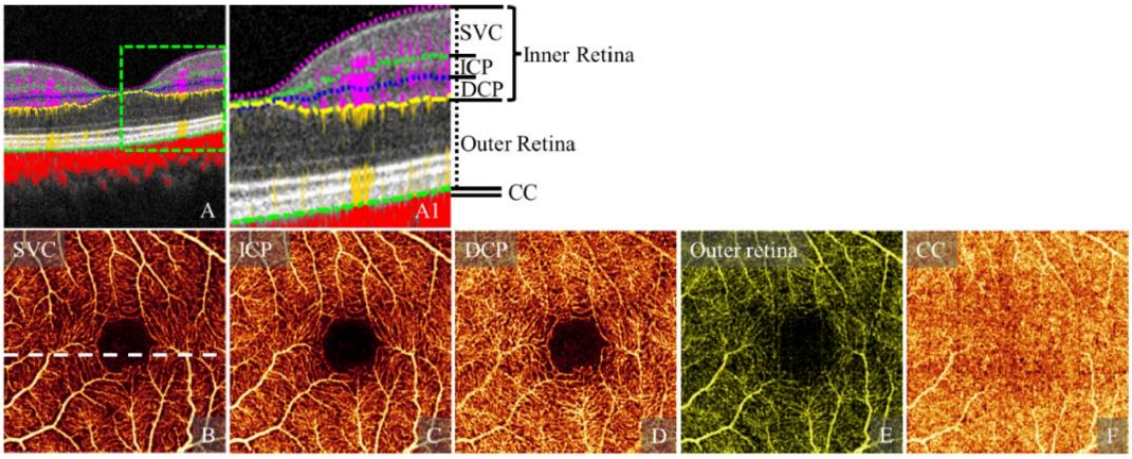


Figure 2. Typical projection artifacts in OCTA. These artifacts appear as "tails" in B-scan images and duplication of superficial vascular patterns in deeper en-face images. (**A**) B-scan OCT image overlaid with a color-coded OCTA signal: the inner retina is shown in violet, the outer retina is shown in yellow, and the choroid in red. A magnified view of the green box is provided in (**A1**). (**B**–**F**) En-face OCTA image of various slabs: the superficial vascular complex (SVC) in (**B**), the intermediate capillary plexus (ICP) in (**C**), the deep capillary plexus (DCP) in (**D**), the outer retina in (**E**), and the choriocapillaris in (**F**) [31].

The formation of projection artifacts can be explained by the theory of light scattering and photon propagation in the OCT/OCTA imaging process [32]. The depth resolution in OCT is obtained by the coherent gating principle, which maps the optical path length of the detected photons to the anatomical position in the retina [24]. Red blood cells are the main scatterers in the vessels, and the interaction of incident photons with moving red blood cells forms the dynamic contrast of OCTA imaging. The interaction of photons with red blood cells can be divided into two categories: single backscattering and multiple instances of forward scattering and backscattering. Due to the movement of red blood cells, photons that undergo single backscattering will be detected as fluctuating signals over time, and the optical path length in this case is the round-trip distance to the scatterer, which can obtain the accurate position of red blood cells and vessels. Projection artifacts may originate from the multiple times of forward scattering and backscattering of photons, and there are two situations that can produce this type of projection artifact. Figure 3 shows schematic diagrams depicting the two situations of projection artifact formation. The first situation is that the incident photons experience multiple times of scattering before being backscattered by red blood cells and eventually collected. This lengthens the optical path length of the photons, which exceeds the equivalent optical path of the lower boundary of

the vessel, resulting in dynamic signals below the vessel and producing tail artifacts in the B-scan cross-sectional angiography image. The second situation is that the photons passing through the superficial moving red blood cells reach high-reflective static tissue (such as retinal pigment epithelial cell layer) below the vessel, and then undergo backscattering before finally being detected. Due to the flow of blood in the vessel, the motion signal is mapped to the depth of its total path length, rather than to the path length of the moving red blood cell. This kind of light reflection is detected as having dynamic contrast similar to blood flow, which will mimic shallow vascular structures in deep tissues, forming another cause of projection artifacts.

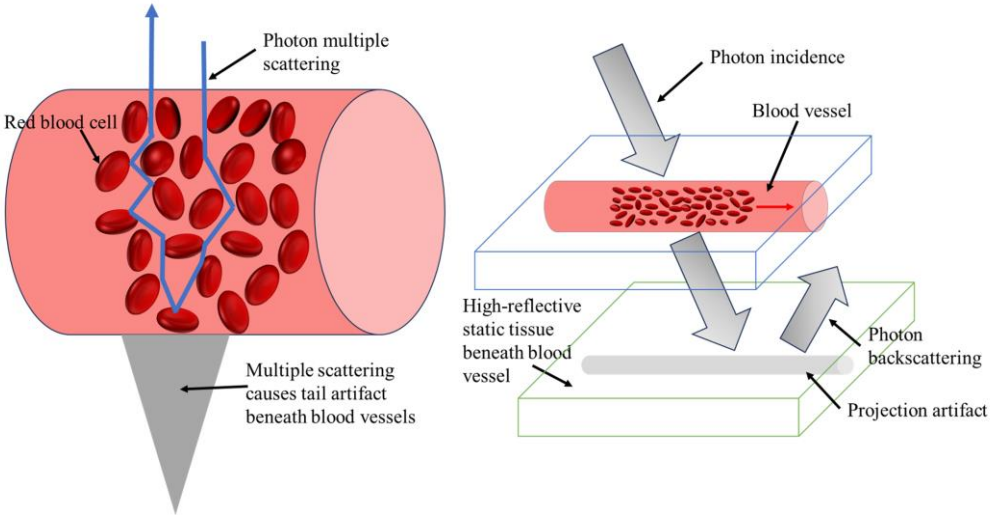


Figure 3. Schematic of projection artifact generation. The left image indicates that photons are scattered multiple times and eventually collected by the objective lens, appearing as false blood flow signals (tail artifacts) below the vessel. The right image shows a photon passing through a superficial layer of flowing red blood cells to reach the highly reflective static tissue below the vessel and then backscattering occurs. In both cases, the projection artifact appears in the tissue below the vessel.

Projection artifacts significantly affect the interpretation and quantification of OCTA. In healthy eyes, the outer retina is avascular, but a projection artifact generates false blood flow signals in the outer retina, which greatly impairs the detection and quantification of neovascularization [18]. Tail artifacts can also obstruct the visualization of retinal vascular proliferation because they can conceal the true proliferative vessels that connect the retinal and choroidal circulation [33]. Furthermore, a tail artifact beneath large vessels compromises the capability of OCTA to achieve true 3D imaging of the vascular network.

Various processing methods have been proposed to suppress projection artifacts. Leahy et al. [34] proposed a hardware-based OCTA method, which uses a high numerical aperture (NA) objective lens with a short depth of focus in the OCT system to acquire OCTA data. This provides a very thin detection layer so that photons that experience multiple scattering and end up outside the detection layer will not be collected by the objective lens, thus suppressing the tail artifact below the vessel. However, this method requires multiple scans at different depths, which greatly increases the data acquisition time. A more popular method to suppress projection artifacts is to utilize signal processing algorithms. The slab subtraction algorithm is a processing method that subtracts the weighted angiography signal of shallow tissue from that of deep tissue in en-face imaging of different retinal layers [6,35]. This method is simple to operate and has the advantage of significantly removing projection artifacts, but the disadvantage is that it may disrupt the continuity of the vascular network in deep tissue, bring shadowing artifacts, and cause their vascular density to be underestimated. To minimize the interruption problem based on axial subtraction, Zhang

et al. [36] further proposed a projection removal (PR-OCTA) algorithm, which is based on a normalized OCTA intensity signal. It finds the local peak of normalized blood flow signal along each A-scan to eliminate false blood flow and preserve true blood flow. Experimental results showed that this method better preserved true blood flow under shallow vessels while eliminating projection artifacts and improved the continuity of the deep vascular layer. Subsequently, Wang et al. [37] proposed a reflection ratio-based projection removal (rbPR-OCTA) algorithm, which further improves blood flow continuity by simultaneously taking OCT structural reflection signal into consideration. It demonstrated that true blood flow in deep tissue corresponds to a brighter reflection signal on OCT structure, while projection artifacts correspond to a lower reflection signal. Using this feature, it obtains a more accurate vascular contrast map and vascular probability distribution map to detect and remove tail artifacts and enhance vascular continuity. Wang et al. [31] propose a signal attenuation-compensated projection-resolved OCTA (sacPR-OCT) algorithm. This approach estimates the magnitude of projection artifacts while accounting for signal attenuation. Through signal attenuation compensation, this method effectively eliminates projection artifacts and enhances the true flow signal beneath large vessels. Figure 4 illustrates OCTA imaging of a normal eye, presenting a comparison of multiple retinal layers before and after utilizing different projection artifact processing algorithms. Shape-based filtering methods (such as Hessian filtering) have also demonstrated the ability to suppress tail artifacts in OCTA. For instance, Yousefi et al. [38] combined multi-scale 3D Hessian filtering, intensity-based segmentation, and morphological segmentation techniques to achieve more accurate angiography and vessel segmentation. Li et al. [39] introduced an adaptive classifier based on 3D Hessian filtering to enhance OCTA data. It uses a Gaussian probe kernel in the vertical direction to detect and remove vessels with long tail artifacts while preserving vessels with short tail. These shape-based filtering methods can minimize tail artifacts. Tang et al. [40] proposed a normalized field autocorrelation function-based OCTA (g1-OCTA), which incorporates repeat A-scan acquisition along with dynamic analysis to mitigate blood vessel tail artifacts in OCTA imaging. The g1-OCTA method employing a shorter decorrelation time was found to be effective in suppressing the blood vessel projection artifacts. However, they also concluded that implementing this shortened decorrelation time inadvertently attenuates microvascular signal strength. Subsequently, Zhou et al. [41] devised an adaptive g1 analysis-based technique (Ag1-OCTA) to tackle these issues. Their method adaptively applies a short decorrelation time to voxels prone to projection artifacts while employing a longer decorrelation time for vessel voxels. The results demonstrate significant suppression of projection artifacts under macro vessels and enhancement of dynamic microvessels signals. Recently, deep learning-based methods have also been applied to suppress projection artifacts. Stefan et al. [42] proposed a deep learning method, which uses manually labeled ground truth of vascular structure to divide OCTA volume data into multiple small 3D volume blocks for training. It uses a neural network encoder–decoder to enhance vascular information, which can suppress tail artifacts and enhance vascular connectivity. However, the limitation of this deep learning-based OCTA enhancement technique is that it requires high quality label data for model training. It is believed that along with their fast development, increasingly powerful deep learning methods will be adopted in this field to solve the complicated projection artifact problem of OCTA in the future.

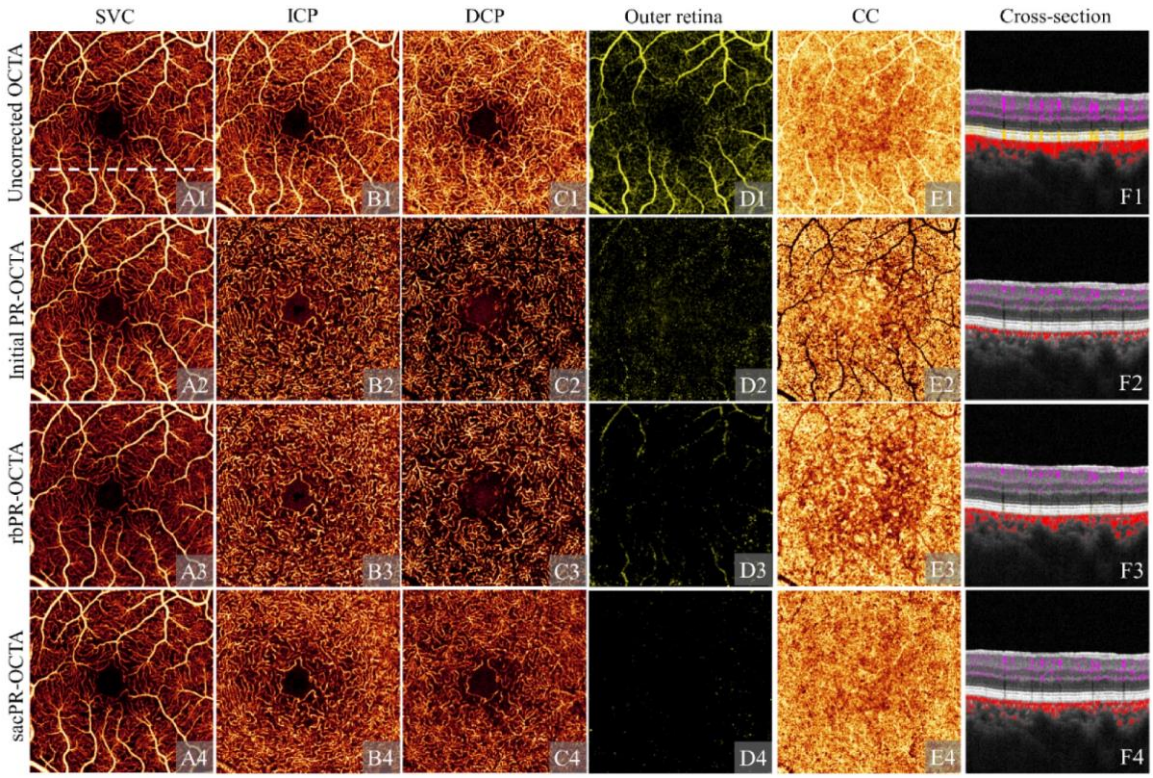


Figure 4. Images of a normal eye captured using uncorrected OCTA (Row 1), initial projection-resolved OCTA (PR-OCTA; Row 2), reflectance-based projection-resolved OCTA (rbPR-OCTA, Row 3), and the signal attenuation-compensated projection-resolved OCTA (sacPR-OCTA, Row 4) are presented. The images depict en-face OCT angiograms of the superficial vascular plexus (SVC, column A), the intermediate capillary plexus (ICP, column B), the deep capillary plexus (DCP, column C), the outer retina (column D), and the choriocapillaris (CC, column E). Additionally, column F displays typical cross-sectional structural OCT overlaid with color-coded flow signal (violet: inner retina, yellow: outer retina, red: choroid) at the position indicated by the white dotted line in A1 [31].

3.1.2. Weak Signal Artifact

A weak signal artifact refers to a type of OCTA artifact induced by a weak OCT signal. Two situations will lead to a weak OCT signal: the first one includes an abnormal occurrence of high-density media in the propagation path, and the second one is related to a large accumulated path attenuation that makes the signal as low as the noise. These two artifacts are called masking artifacts and attenuation artifacts, respectively.

A masking artifact refers to the local signal loss of the underlying tissue due to obstruction caused by the existence of some high-density media on the upper layer during OCTA imaging, which is manifested as blood flow shadow areas in en-face angiography, hence also being called a shadowing artifact [43]. Figure 5 shows the en-face OCTA images with and without shadowing artifacts [44]. Masking artifacts are usually attributed to OCT signal loss induced by its upper high-density media, which may be associated with retinal pathology, such as retinal hemorrhage, subretinal fluid, or result from features outside the retina, such as vitreous floaters, vitreous hemorrhage, corneal opacity, pigment clumps, and mature cataract. Even in healthy human eyes, large vessels in the retina can also cause shadowing artifacts [45]. In addition, the slab subtraction algorithm used to remove projection artifacts can also introduce masking artifacts [35]. In wide-field OCTA imaging, masking artifacts caused by eyelashes are also common [46].

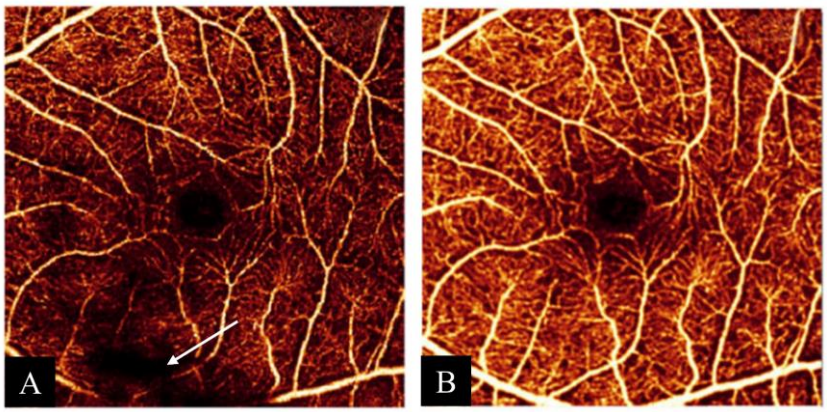


Figure 5. Shadowing artifact. (**A**) Retinal en-face OCTA before vitrectomy with obvious shadowing artifacts (arrow) caused by vitreous floaters; (**B**) retinal en-face OCTA after surgical removal of vitreous floaters. Full vascular networks are visible without shadowing artifacts [44].

Masking artifacts can significantly affect any vessel-related measurement and may impede the monitoring of other pathological developments. If the artifact occurs in the area of neovascularization, it will severely compromise the visualization of retinal microcirculation. The depth of penetration in OCT systems is affected by the center wavelength of the light source. Longer wavelengths generally experience less optical attenuation compared to shorter ones, and therefore systems with longer wavelengths can help mitigate the effects of masking artifacts [47]. A study conducted by Reich et al. [48] compared imaging techniques using SS-OCTA with a 1050 nm wavelength and SD-OCTA with an 840 nm wavelength. Because of longer wavelength and better sensitivity roll-off characteristics, SS-OCTA had a deeper light penetration and improved vessel visualization in deeper tissue layers compared to the SD-OCTA in this study. Generally, SS-OCTA with a longer wavelength could potentially diminish scattering and absorption caused by subretinal fluid and could lessen but not completely eliminate the shadowing artifact. For masking artifacts caused by vitreous floaters, the results of two scans can be combined to form a complete OCT and OCTA image, since the shadow normally does not overlap between the two scans when the floaters move due to eye saccades [44]. Shadow areas caused by vitreous floaters may be confused with non-perfusion areas (NPAs) on en-face OCTA. However, NPA areas usually maintain normal intensity OCT structural signal, so masking artifacts and NPA can be distinguished by checking whether the OCT signal intensity is reduced [49]. Camino et al. [44] trained an ensemble classifier to automatically identify shadow areas using random forests, which could classify shadow areas accurately. Convolutional neural network (CNN) is a deep learning technique that has been rapidly developing in recent years. Guo et al. [19] integrated CNN with U-Net-like architecture into their NPA classification algorithm, which was proven to distinguish NPA and shadowing artifact reliably.

Noise-induced blood flow signals may arise when the OCT signal is weak. These signals are detected by many OCTA motion contrast algorithms as noise fluctuations, resulting in false blood flow signals. To remove false OCTA pixels produced by noise signal fluctuations, a thresholding operation may be applied in OCTA data processing. The principle of thresholding is that only OCT signals above a certain intensity threshold will be considered in generating OCTA flow signals. This image artifact, where the real OCTA blood flow signal is obscured by low-signal regions, is termed an attenuation artifact [47]. Figure 6 shows the appearance of attenuation artifacts at different thresholds [47]. Attenuation artifacts are caused by the system processing weak signals, while the masking artifacts are caused by the loss of OCT signal due to light occlusion.

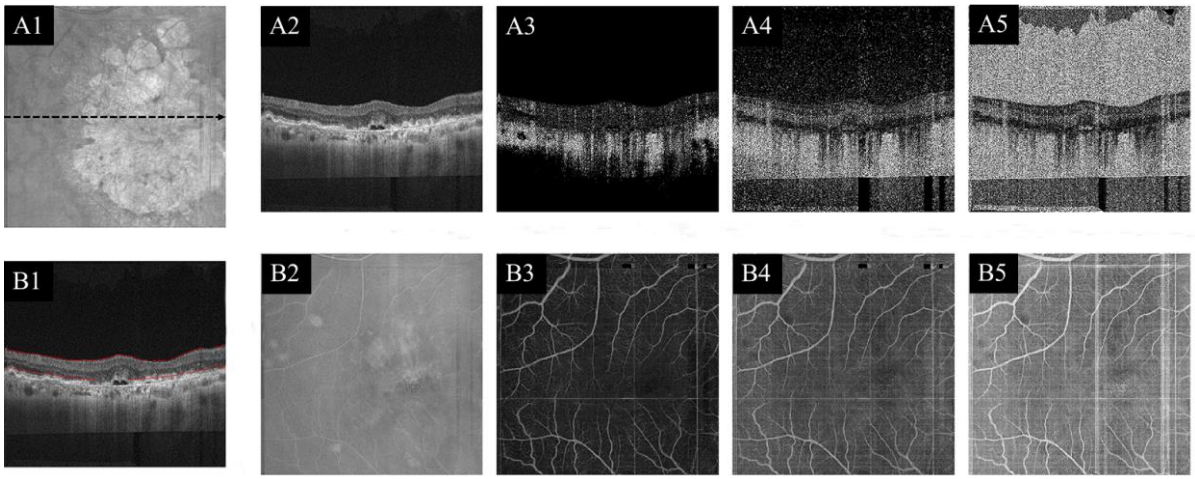


Figure 6. Attenuation artifact. (**A1**) En-face OCT using average projection of the entire retina. (**A2**) OCT B-scan at the dashed black line in A1. (**A3**) B-scan OCTA image with a threshold of mean + 6 × standard deviation (SD) of the noise signal intensity. (**A4**) B-scan OCTA at a threshold of mean + 2 × SD of the noise signal intensity. (**A5**) B-scan OCTA without thresholding. (**B1**) The OCT B-can image at the dashed line of (**A1**). The two red lines indicate the retinal layer for the en-face images of (**B2**–**B5**). (**B2**) En-face OCT image. (**B3**) En-face OCTA image with a thresholding of mean + 6 × SD of the noise signal intensity. (**B4**) En-face OCTA image with a threshold of mean + 2 × SD of the noise signal intensity. (**B5**) En-face OCTA without thresholding. A high-value thresholding masks the flow area with a low OCT signal, while low-value or no thresholding will produce a lot of noise-induced artifacts [47].

OCT signal attenuation can be caused by various factors during OCTA data acquisition, such as scanning defocus, medium opacity, pupil vignetting, system aberration, and signal roll-off [22]. These factors can degrade image quality, impair vascular details visualization, and even generate false blood flow information. Vignetting is one of the common causes of low signal in large field-of-view OCTA imaging. It occurs when the incident light beam is partially blocked by the iris, resulting in reduced illumination of the retina. Vignetting can be induced by a large beam, small pupil, or instrument-eye misalignment. Misalignment can cause a significantly increased scanning angle, which broadens the low signal area [50,51]. Besides vignetting, cataract and tear film rupture can also lead to an increase in overall signal attenuation. Damaged tear film can diminish the eye's focusing ability, making the image darker. The overall signal loss of the image can compromise the accuracy of OCTA measurements, such as vascular density measurement. Yu et al. [52] found that vascular density varied by about 10% in imaging the same eye under different signal strength conditions. Smaller vessels are also hard to display in low signal areas because their blood flow signals are comparable to noise intensity, which may be neglected in background noise processing. The presence of attenuation artifacts affects the interpretation of OCTA images. It is essential to recognize that the absence of an OCTA signal does not necessarily mean there is no blood flow. Analyzing both OCT and OCTA images together is critical to verify the accuracy of the OCTA signal. De et al. [51] proposed three approaches to detect attenuation artifacts on OCTA images, namely the cross-sectional method, the en-face method, and the orthogonal plane method. These three strategies can identify and evaluate the low signal situation in the region of interest. Gao et al. [53] effectively eliminated the impact of signal strength on vascular density measurement by compensating for reflectance variation. Additionally, both traditional image filtering and modern machine learning-based image enhancement can be used to highlight vascular system imaging and reduce the impact of low OCT signal [54].

3.1.3. Unmasking Artifact

Unmasking artifacts, also called exposure artifacts, refer to the imaging defect that occurs when the OCT structural signal is locally enhanced due to increased OCT signal penetration rate in some areas with pathological lesions, such as the retinal atrophy or retinal pigment epithelial (RPE) atrophy. This makes the local vascular network appear brighter than the surrounding part [55]. Unmasking artifacts resemble a neovascular complex, which may result in inaccurate measurement, compromise the accuracy of the automatic vessel segmentation algorithm, and even lead to misdiagnosis of pathology [56]. Figure 7 shows the unmasking artifacts both in en-face and B-scan OCTA images [43].

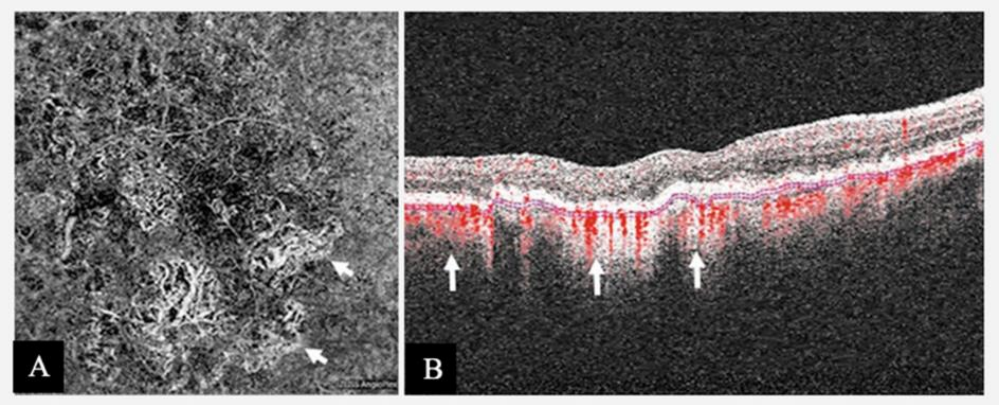


Figure 7. Unmasking artifact. (**A**) En-face OCTA of a patient with geographic atrophy (GA) shows brightened choroidal vessels (arrows) due to unmasking artifacts, which may be confused with choroidal neovascularization. (**B**) B-scan shows a choroidal structure signal overlaid with red blood flow signal (arrows indicate exposed blood flow signal) [43].

OCTA signal may exhibit unmasking artifacts in eyes affected by diseases such as age-related macular degeneration (AMD). Falavarjani et al. [56] reported that 9 out of 57 eyes (15.8%) showed exposure artifacts, including 6 eyes with AMD-induced geographic atrophy (GA) and 3 eyes with both choroidal neovascularization (CNV) and GA. In the B-scan OCTA images, the regions with exposure artifacts corresponded to the regions of RPE atrophy. This was attributed to the increased light transmission through the areas of RPE atrophy, which enhanced the OCT signal intensity of the underlying choroid. The blood flow perfusion in these regions is more discernible than that in the adjacent tissues, leading to a potential misdiagnosis of CNV. A combination of en-face and B-scan OCTA images can help differentiate unmasking artifacts from true CNV [57].

3.2. Motion Artifacts

3.2.1. Eye Movement Artifact

OCTA signal is formed by detecting pixel change between repeated B-scans using either absolute or relative change calculation [47]. During image acquisition, the movement of the subject's eye relative to the device will cause a motion contrast signal in the entire B-scan, which forms a false blood flow signal. This artifact is called an eye movement artifact [58]. Figure 8 shows the typical eye movement artifacts, which appear as white lines and blood flow displacement in the en-face image [59].

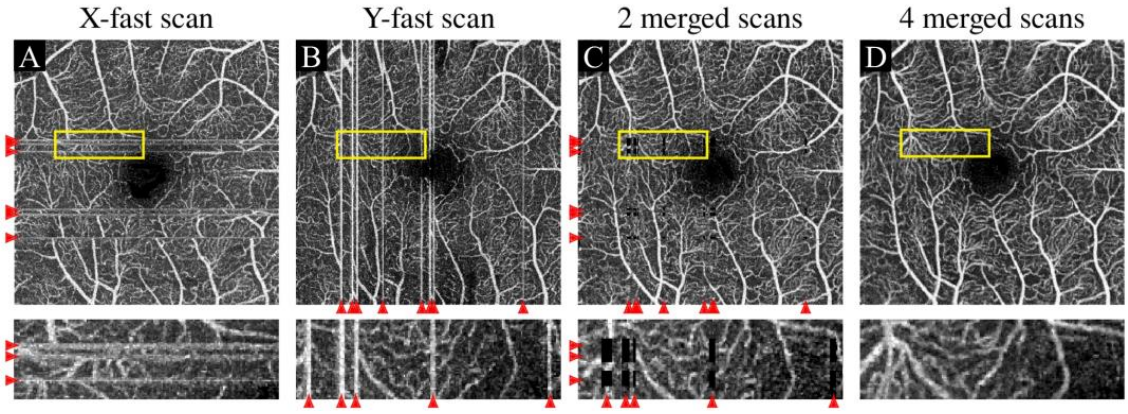


Figure 8. Typical examples of eye motion artifacts and OCTA images after motion correction are shown. Red arrows point to bright white lines in original scans, with zoomed images displaying enlargements of the yellow rectangles. (**A**) Original X-fast and (**B**) Y-fast scans exhibiting white line artifacts and blood vessel displacement. (**C**) Merged volume from one pair of orthogonal scans with B-scans corresponding to white lines excluded, resulting in data gaps represented as black boxes where the removed B-scans intersect. (**D**) Merged volume from two pairs of orthogonal scans (totaling 4), effectively filling the data gaps [59].

Eye movement can be classified into two types, depending on whether it is caused by external or internal factors. External eye movement involves local rotation of the eye by extraocular muscles and global movement of the eye by head, neck, and body movement. It also includes slow eye drift movement [60]. Internal eye movement results from heart beating, breathing, tremors, and microsaccades, which create pulsation in the eye. Microsaccades happen every few seconds, which coincide with the time scale of OCTA data acquisition. Therefore, microsaccades can affect multiple B-scans, leading to bright white lines on the en-face OCTA image [23], which disrupt or spatially shift the vessels.

Axial motion of the retina and choroid is also common in OCTA data acquisition, which is visible in volumetric data. A method to minimize the effect of axial motion is to register or align successive B-scan images [61]. Some OCTA image processing algorithms, such as split-spectrum amplitude-decorrelation angiography (SSADA), decrease the sensitivity to axial eye motion by reducing the axial resolution, and then average multiple lower-resolution images in each spectral sub-band to enhance the signal-to-noise ratio of angiography [26]. These methods can alleviate the problem caused by axial motion.

Lateral eye motion is an important source of eye movement artifacts in OCTA images. There are both hardware and software-based solutions to address the problem of lateral eye motion. Hardware processing solutions usually rely on adding auxiliary imaging techniques (such as scanning laser ophthalmoscopy) to track eye movement [62,63], and there are also algorithm-based studies that use only OCTA data without additional hardware for eye movement artifact correction [46]. It is worth noting that both software and hardware-based methods have their advantages and drawbacks. The choice between them depends on the specific application requirements and they can also be implemented in one system simultaneously to achieve the best imaging performance. Real-time tracking systems temporarily stop scanning when eye motion is detected during OCTA acquisition and then restart the scanning at the affected position when the motion stops, through which the eye motion effect is avoided [64,65]. Although this method may increase the imaging time, it can reduce the artifacts caused by eye motion relatively well. In software-based processing, if multiple scans are available, they can be registered and merged to restore the B-scan lost in a single scan, whereas multiple scans can also be used to enhance image quality through averaging [66]. For example, Zang et al. [60] used parallel stripe registration in multiple

consecutive scans of the same area to fuse the obtained images to remove eye movement artifacts. Data from two orthogonal fast scan directions (e.g., in an orthogonal raster scan scheme, acquiring an X-axis fast scan OCTA volume data and a Y-axis fast scan OCTA volume data separately) can also be registered to achieve complimentary information and eliminate eye movement artifacts [67]. Camino et al. [68] proposed a regression-based block motion removal technique to suppress slow eye movements (eye pulsation and drift). The algorithm divides OCTA B-scans into segments, analyzes the bulk motion velocity within each segment using linear regression, and calculates a reflectance-adjusted threshold for bulk motion decorrelation. It subtracts bulk motion velocity from flow voxels using a nonlinear decorrelation–velocity relationship. This method achieved an improved OCTA imaging with bulk motion noise cleanup compared to the simple median-subtraction method.

In addition to these traditional image processing methods, the recently fast-developing artificial intelligence-based image processing can also be used to remove eye movement artifacts [45]. Hossbach et al. [69] trained a U-Net convolutional neural network using corresponding OCT and OCTA volumes. They used the trained network to generate OCTA images from a single OCT image, which was then used to replace the original OCTA images affected by eye movement artifacts. This approach demonstrated its capability to suppress eye movement artifacts while preserving partial blood flow information. However, due to the use of a single structural image from a specific location which lacks a motion contrast mechanism for blood flow calculation, the generated OCTA images may exhibit some degree of information loss and reduced vessel continuity in en-face OCTA images.

3.2.2. Banding Artifact

Banding artifacts appear as wide bands of different brightness on the OCTA images of various retinal layers [70]. This artifact may be induced by the change in distance between the subject and the device during data acquisition, caused by motion or by the change in acquisition angle or light intensity lasting for a certain while, which makes the reflection intensity vary between adjacent B-scans. Eye movement correction software sometimes introduces another artifact, called a quilting artifact (or checkerboard artifact, crisscross artifact). Quilting artifacts are caused by insufficient correction of multiple scans in vertical and horizontal directions [61], i.e., eye movement will produce signal gaps in each volume of data, where some areas of the retina are not imaged. These gaps appear as horizontal or vertical black lines in the image, creating a staggered rectangular-shaped artifact similar to quilting lines [47]. Lauermann et al. [70] considered quilting artifacts and banding artifacts to be the same artifact. Figure 9A,B show the typical banding artifact [71] and quilting artifact [19] in en-face OCTA images.

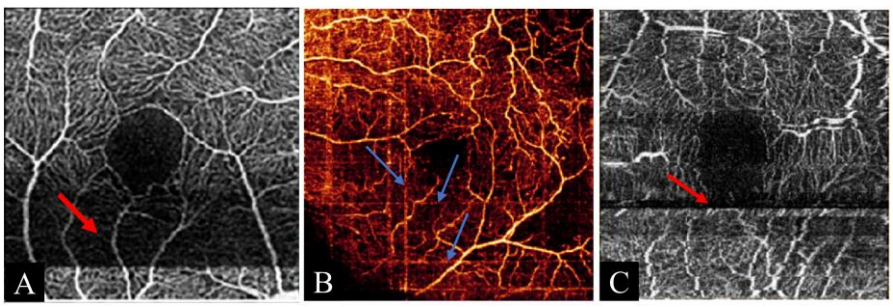


Figure 9. Banding artifact, quilting artifact and blinking artifact. (**A**) Banding artifact shown as a band with different brightness (arrow) [71]. (**B**) Quilting artifact shown as vertical or horizontal thin lines (arrows) [19]. (**C**) Blinking artifact typically shown as an end-to-end black line (arrow) in the en-face OCTA image (arrow) [71].

Banding artifacts vary in each segmented layer and are more prevalent in the superficial and middle layers of the retina, and less common in the deeper retina layers [72]. Banding artifacts degrade the image quality of OCTA, lower the repeatability of vascular density measurement, and reduce the visibility of capillary structure in the affected area [73]. Recent OCTA systems use fast and accurate tracking software to effectively prevent banding artifacts [56].

3.2.3. Blinking Artifact

The blinking artifact occurs when the subject blinks during image acquisition, causing the B-scan signal to be absent during blinking. This leads to the creation of a black line of varying widths across the en-face angiography images of all retinal layers. The width is determined by how long the blinking lasts [70]. Figure 9C shows the typical blinking artifact in OCTA images [71].

Blinking artifacts are common artifacts in OCTA [74], and it can be avoided simply by not blinking during scanning. Therefore, it is crucial to instruct the subject to cooperate during the data acquisition process. It is good practice to encourage the patient to blink several times right before scanning in order to ensure homogeneous tear film distribution and achieve high scanning quality. Blinking frequency is influenced by many factors for individuals, and some studies have found that dry eye and vision degradation can increase the patient's blinking frequency significantly and severely disturb image acquisition [22,55].

Faster image acquisition speed or eye-tracking software can help reduce blinking artifacts [27]. For example, Wei et al. [46] designed an OCTA system with a built-in eye motion tracking system. It detected each blink by calculating the instantaneous motion index during data acquisition and rescanned right after the eye reopened, which could effectively solve the problem of blinking artifacts.

3.2.4. Fringe Washout Artifact

Fringe washout artifacts occur in choroidal OCTA, which is caused by phase instability due to fast red cell motion in big choroidal vessels, leading to interference fringe washout effect. The choroidal vessels have poor backscattering signal from blood flow, resulting in a blurring effect [75,76]. Retinal vessels produce higher OCTA signals than the surrounding tissue, while choroidal vessels are different from the retinal vessels. The fringe washout effect hinders the display of high blood flow signal in the choroidal vessel, which appears dark in contrast to the surrounding stroma where bright flow signals are present. The fringe washout effect can also be caused by axial sample motion, which reduces the imaging depth and image signal-to-noise ratio. Faster imaging speed can help avoid fringe washout effect in OCT imaging [77,78] but a balance between sampling speed and spectrometer detection sensitivity should remain to keep a high enough signal-to-noise ratio in imaging. Figure 10 shows the typical appearance of fringe washout artifacts in choroidal OCTA images [79].

3.3. Improper Operation Artifacts

These types of artifacts occur when the operation of the relevant technicians or subject cooperation is improper. Usually, these artifacts can be avoided or reduced by good device operation training and subject education, and by re-performing the correct operation if there is any abnormality encountered in the OCTA data acquisition process.

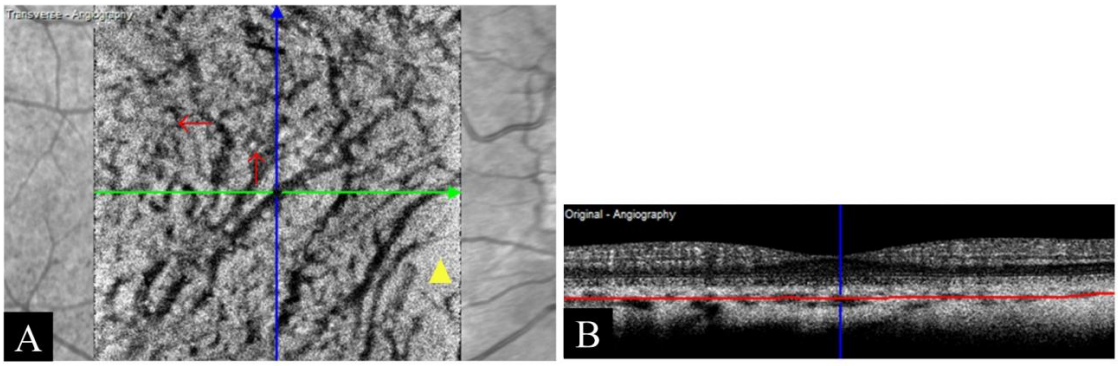


Figure 10. Fringe washout artifact. (**A**) En-face OCTA shows choroidal stroma with high blood flow signal (yellow arrow) and dark vessels (red arrows) due to fringe washout artifact. (**B**) OCTA B-scan at the cross-section of the green line in (**A**) shows choroidal vessels appear as low flow signal [79].

3.3.1. Defocus Artifact

Defocusing occurs when the scanning areas are outside the region of focus. In this situation, the overall intensity of the B-scan is reduced, resulting in blurred large vessels and reduced or disappeared microvessels on the en-face OCTA image, which is called a defocus artifact [80,81]. Defocusing also occurs in part of the scanning areas due to improper angle adjustment or abnormal curvature of the scanned tissue such as the eye with high myopia. A part of the image presents a defocus artifact caused by a tilted acquisition angle, which is called a tilt artifact [74]. Figure 11 shows the defocus artifact [82] and tilt artifact [83] in en-face OCTA images.

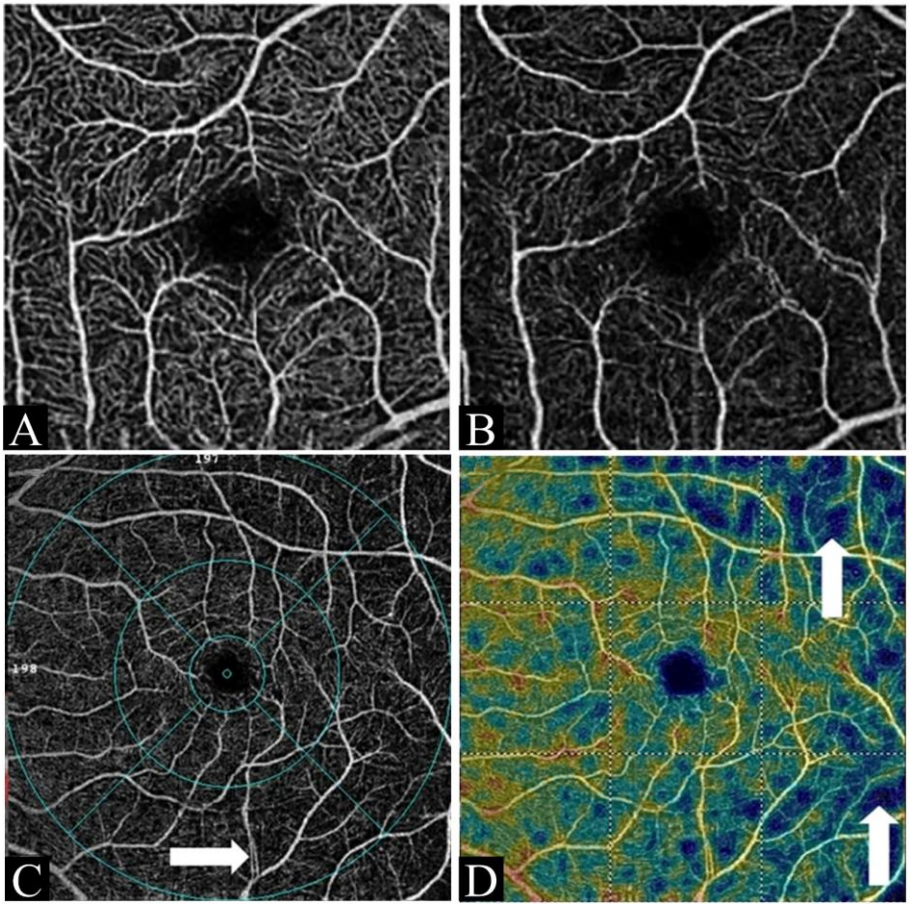


Figure 11. Defocus artifact and tilt artifact. (**A**) En-face OCTA image with good focus [82]. (**B**) En-face OCTA image with defocus artifacts. Large blood vessels are blurred, and visibility of small blood vessels

is reduced or even lost [82]. (**C**) Tilt artifact. Right part of the OCT scan is out of focus, reducing visibility of vessels on this side of the image [83]. (**D**) En-face OCTA image with vascular markings and vascular density map in correspondence to (**C**), the right side of the image shows reduced vascular density due to tilt artifacts (vertical arrows) [83].

Defocus artifacts cause blurring or signal loss of OCTA image vessels, which may greatly underestimate vascular quantitative evaluation. These artifacts can be alleviated by careful operations including correctly adjusting the acquisition angle and accurate placement of the location of focus [84].

3.3.2. Mirror Artifact

Mirror artifacts, also called inversion artifacts, occur when the image folds around the reference zero delay line. This artifact happens in both Fourier domain (FD) OCT systems including spectral domain (SD) OCT and swept source (SS) OCT [27]. FD OCT generates images with reference to the zero-delay line, but the device cannot distinguish between negative and positive time delays, so the images around the zero-delay line are usually mirrored. Figure 12A shows the typical mirror artifact in B-scan OCTA [81].

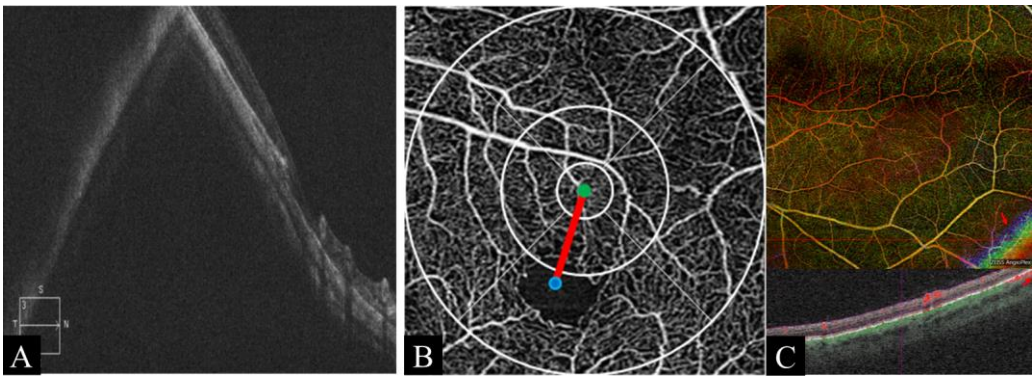


Figure 12. Mirror artifact, decentration artifact, and Z-offset artifact. (**A**) Mirror artifact, which takes place for areas crossing the zero-delay line [81]. (**B**) Decentration artifact. The fovea is not at the center of the en-face OCTA [85]. (**C**) Z-offset artifact. Red arrows show signal errors due to part of the retina placed out of the top edge of the scan window. Depth encoding errors and flow signal errors are seen in the en-face depth-encoded OCTA images [72].

Mirror artifacts are more likely to occur in eyes with high curvature (e.g., high myopia) or elevated lesions, such as those seen in neovascular AMD, choroidal tumors, or retinal detachment [81]. The scanned retinal surface may be placed too close to the zero-delay line, or the scan may be too tilted, both leading to mirror artifacts. Mirror artifacts can cause errors in retinal layer segmentation and affect accurate image interpretation. To reduce mirror artifacts, effective strategies include increasing the axial scan depth range, performing additional scans to center the area of interest, or using post-processing algorithms for correction [86].

3.3.3. Decentration Artifact

A decentration artifact is a kind of scanning error artifact when it is required for fovea-centered retinal OCTA applications. It happens when the fovea is not in the center of the en-face OCTA image, or even outside the scan area, because of eye movement or camera misalignment. In this case, the subsequent OCTA image processing algorithm may fail to recognize the fovea correctly [75]. Decentration artifacts can affect macular thickness measurements [87]. In addition, this can cause problems in segmenting the retinal fovea, as

some algorithms use the image center as the initial boundary or use a distance function based on the OCTA image center as the input. They may produce incorrect results due to decentration artifacts, which can affect the measurement of the fovea area [88]. Figure 12B shows the typical decentration artifact [85].

3.3.4. Z-Offset Artifact

A Z-offset artifact occurs when the subject head is not positioned correctly, leading to vertical shifts of cross-sectional OCT scans within the OCT image window. This causes some regions of the retina to appear outside the scanning range, also known as out-of-window artifacts. The OCT B-scan images reveal that some retinal regions extend beyond the OCT window [84]. This artifact is manifested as a loss of vascular signals in some areas in en-face OCTA [72,80]. The degree of Z-offset artifact is related to the proportion of the B-scans that have partial retinal regions outside the OCT window. This error is often due to operation errors and can be fixed by aligning the scan with the center of the frame [89]. Figure 12C shows the typical Z-offset artifact in OCTA [72].

3.4. Signal Processing-Related Artifacts

Common OCTA signal processing for fundus imaging mainly includes generating blood flow signals from repeated OCT structural images and then performing en-face projection imaging according to different retinal layers. Therefore, retinal layer segmentation is required in advance. This section mainly describes the artifacts caused by improper or incorrect signal processing in the generation of en-face images. It should be pointed out that in the process of generating blood flow signals from structural OCT signals, some improper operations such as using too low OCT threshold signals to mask OCTA blood flow signals will also cause artifacts, such as the attenuation artifact described in Section 3.1.2.

3.4.1. Segmentation Error Artifact

En-face projection is a widely used OCTA imaging technique that can be used to show the blood vessels of various retinal layers. To create an en-face image for a specific layer, one needs to segment, i.e., to find the two boundary edges of the specific retinal layer precisely, in order to facilitate the statistical (such as the maximum or mean) signal strength calculation along the depth axis in this layer. If the segmentation algorithm produces incorrect lines, the en-face OCTA image will display inaccurate blood flow data, resulting in segmentation error artifacts [80]. Figure 13 shows the segmentation error artifacts caused by incorrect placement of retinal segmentation lines, which generate misleading blood flow images [90].

An incomplete segmentation error is a frequent type of segmentation error. It happens when part of the layer edge is not segmented properly [91]. Incomplete segmentation errors are more often seen in diseased eyes, although some clinical studies showed that this artifact also appears in normal eyes with Heidelberg Spectralis and Zeiss Cirrus OCT devices [27]. Sometimes, when the segmentation line is totally deviated from the retinal layer edge, it is called a complete segmentation error. Complete segmentation error is rare and only shows up when all the retinal layer structure is severely damaged [91].

Accurate OCTA results depend on correctly recognizing the layers of the retina and choroid. Wrong segmentation creates en-face OCTA images that differ from the actual anatomy. Spaide et al. [92] demonstrated that segmentation errors affect OCTA quantitative measurements. The capability of retinal layer segmentation software is not guaranteed, i.e., it cannot obtain 100% accuracy. Computer algorithm-based automatic segmentation algorithms heavily rely on the histological structure of the retina. The normal retina has distinct but regular texture variations in its structure, and the segmentation algorithm can usually work reliably. But various anomalies are seen in cases of automatic segmentation

of diseased retina [61]. The algorithm developed on the basis of a healthy retina normally cannot segment the layers of diseased eyes accurately and reliably. Ocular pathologies include various complex lesions such as edema, cysts, subretinal fluid, pigment epithelial detachment, neovascularization, and atrophy [61], which cause the algorithm to generate segmentation error artifacts [43]. For instance, there are structural anomalies like tilting, stretching, or dragging in myopic eyes that make accurate segmentation very difficult [93]. Segmentation errors are also found to be common in eyes with age-related macular degeneration (AMD) [94].

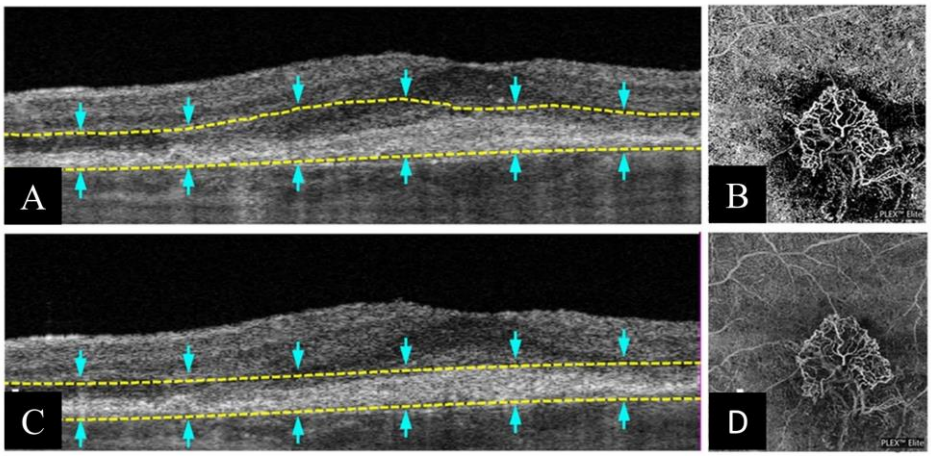


Figure 13. Segmentation error artifact, which is incorrect blood flow shown on en-face OCTA due to segmentation errors. (**A**) B-scan image with incorrect layer segmentation as shown in yellow dotted lines. (**B**) Misidentification of the outer retina to choriocapillaris in a subject with macular neovascularization leading to incorrect en-face OCTA image. (**C**) B-scan image with correct layer segmentation lines generated after manual modification. (**D**) A correct en-face OCTA image [90]. Arrows indicate manually adjusted positions anterior and posterior to any suspected macular neovascularization.

To provide flexibility, the segmentation software from many OCT instrument manufacturers allows operators to correct segmentation errors manually in targeted B-scans. For diseased eyes, it is usually necessary for the operator to adjust the retinal boundary segmentation manually in some OCT B-scans before OCTA image generation and analysis. But this increases the processing time and affects the efficiency of this technology in clinical applications [47]. Many researchers have researched various methods to improve the performance of automatic retinal segmentation algorithms to fit high application demands.

The earliest retinal layer segmentation algorithm identifies the image features in the axial reflection profile and associates them with anatomical structures [95,96], such as those threshold-based, edge-based, region-based segmentation, and axial reflection intensity-based segmentation methods based on single A-line OCT scanning. These methods are reported to have achieved satisfactory retinal layer segmentation results using their own data; however, it is not easy to generalize these methods in various types of clinical OCT images with a low signal-to-noise ratio or lesions of complicated structure. Facing these challenges, nowadays it also becomes a trend to segment retinal layers using deep learning approaches. Many studies utilize classical deep learning models or propose customized models for retinal layer segmentation, achieving promising segmentation results [97–99]. Another segmentation method that is still widely used today is the graph search. One advantage of the graph search is that it can refine the edges produced by other methods [100,101]. For example, Zhang et al. [102] used a semi-automatic segmentation program based on graph search to effectively improve the segmentation performance. In this case, graph search combined with artificial intelligence-based methods achieved satisfactory results [103].

It is also noted that due to image feature differences, one may develop different retinal segmentation algorithms for various anatomical areas. For example, different algorithms for the segmentation of macula [104], optic nerve head [105], or choroid [106] have been developed. It is generally observed that the performance of various retinal layer segmentation algorithms improves along with time, and correspondingly the rate of segmentation error artifact drops gradually. Researchers have also developed specific layer segmentation algorithms in OCT images with different eye diseases such as AMD [107]. General layer segmentation algorithms may fail in these OCT images because retinal structures in these diseases have significantly changed morphologies compared to normal ones. In the case of segmentation for images of an unrecognized disease, the first step of disease classification can also supply important information for layer segmentation. The information on the recognized disease type and the layer edge features of this disease can then be incorporated into the segmentation algorithm to improve its performance [108,109].

3.4.2. Doubling Artifact

Doubling artifacts are common in en-face OCTA imaging where blood vessels appear duplicated or similar in adjacent areas [61]. This artifact is mainly caused by eye movement correction technology (MCT). During eye movement, the MCT algorithm frequently checks the motion area, and the processing of these motion area signals including vessel alignment may cause blood vessels to appear doubled in OCTA images [43]. Figure 14A shows the typical doubling artifact in an en-face OCTA image [110].

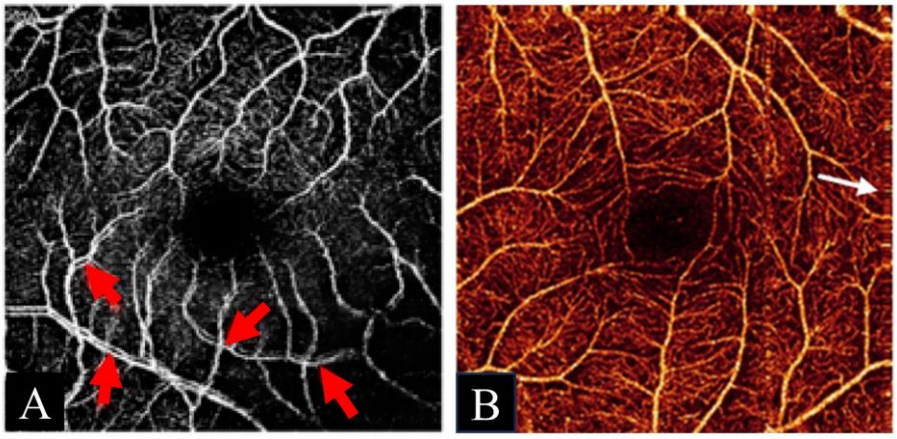


Figure 14. Doubling artifact and stretching artifact. (**A**) Doubling artifact shown as repeated blood vessels (arrows) [110]. (**B**) Stretching artifact, shown as short streaks of varying brightness at the edges of the image (arrow) [64].

A doubling artifact affects the quantitative analysis of dense capillary bed [111], so measures need to be taken to suppress it and make the OCTA image reflect the true blood flow situation. Lauermann et al. [70] compared the OCTA imaging methods with and without eye-tracking technology and found that the doubling artifact occurrence rate of the former was only 3.3%, while that of the latter was as high as 26.7%, indicating that eye-tracking technology can effectively reduce the doubling artifact. However, the correction software itself may also cause additional doubling artifacts. Therefore, doubling artifacts occur with eye movement, no matter whether eye tracking is used [112]. Doubling artifacts have the characteristic appearance of morphologically identical vessels in adjacent regions and a two-phase deep learning framework incorporating detection and removal could be designed to process these doubling artifacts. Synthesized images could be generated manually by adding position-displaced images to raw images, and they are combined as image pairs for deep learning network training.

3.4.3. Stretching Artifact

A stretching artifact is also a related defect caused by the eye movement correction software of the system. Some areas of the en-face OCTA image are stretched and show short stripes of different brightness at the edge of the image. Therefore, it is also known as edge replication [61,70]. This artifact is caused by small angle changes in the focus, resulting in intermittent loss or gain of the signal, which leads to errors in image interpretation [43,113]. Figure 14B shows the typical stretching artifact at the edges of the en-face OCTA image [64].

The occurrence of stretching artifacts is also affected by MCT, which causes line distortion due to interpolation errors in the process of registering and merging OCTA data. Orthogonal grating scanning requires two times of data acquisition, and the motion between these two volume data acquisitions causes the data at the edge of the image to be incorrectly registered, resulting in a stretching artifact [64]. Camino et al. [65] proposed a new method using a registration and selective merging algorithm with a vascular filter, which can automatically detect and eliminate residual stretching artifacts and enhance the visibility of retinal vessels. The complete elimination of this artifact will depend on the future development of MCT.

4. Artificial Intelligence for OCTA Artifact Processing

Artificial intelligence (AI) refers to technologies that enable machines or computers to perform tasks that typically require human intelligence. Within AI, machine learning (ML) is a foundational branch, and deep learning has emerged as a core technique in modern ML applications. In medical image processing, AI, especially leveraging deep learning algorithms, can perform various tasks such as image denoising and super-resolution, thereby enhancing the quality of medical images. These AI algorithms could also be applied to efficiently analyze OCTA images in both research and clinical studies.

With OCTA technology, clinicians can achieve detailed high-resolution observation of ocular vascular morphology, identifying a number of crucial lesions such as microaneurysms, changes in FAZ/vessel density, non-perfusion areas, and neovascularization. This capability enables the applications of OCTA in the diagnosis of a range of posterior eye diseases, including age-related macular degeneration, diabetic retinopathy, retinal vein and artery occlusion, choroidal neovascularization, and polypoidal choroidal vasculopathy [114]. Notably, the integration of AI technology into OCTA analysis facilitates better image processing and disease diagnosis [45,115]. The adoption of DL in OCTA imaging has catalyzed numerous studies focusing on high-quality OCTA image generation, segmentation of clinically useful objects such as vessels, FAZ and nonperfusion area, and various disease classifications. Moreover, advancements in DL techniques tailored for small datasets, such as few-shot learning, have made it possible to extend the application of DL to rare retinal diseases [116]. Recently, AI-assisted OCTA has demonstrated promising capabilities in predicting DR progression [117] or treatment responses to anti-vascular endothelial growth factor therapy [118,119], which has the potential to change the routine clinical practice in disease management [120]. In summary, the integration of OCTA with AI techniques represents a promising frontier in ophthalmic research, with the potential to revolutionize diagnostic capabilities and therapeutic outcomes in clinical applications.

AI for OCTA artifact processing is one of the many abovementioned applications of AI in the OCTA field that has a large potential to significantly improve OCTA image quality. Various applications of AI in OCTA artifact processing have emerged. Table 2 provides a summary of representative AI-based methods for OCTA artifact processing discussed in this section. For light propagation and signal intensity-related artifacts, AI has been used to handle the most common projection artifact, which may include the training of a projection artifact removal network using paired OCTA images. In this approach, the untreated OCTA

image in the pair with tail artifacts is utilized as input, while the counterpart one with manual identification and removal of tail artifact serves as the label in network training. This method results in a framework that can effectively suppress tail artifacts and enhance blood flow continuity [42,121]. Signal intensity-related artifacts exhibit specific features that differ from normal blood flow and non-flow tissue signals. Through extensive data training, AI algorithms can accurately identify these subtle yet crucial features and facilitate further suppression and processing of such artifacts. For instance, Guo et al. [19] proposed a DL network with a U-Net-like encoder–decoder structure to accurately distinguish between non-perfusion areas (NPAs) and shadowing artifacts. Subsequently, precise segmentation of NPA could be performed without the interference of shadowing artifacts. For motion artifacts, Hossbach et al. [69] employed a trained DL model to generate B-scan OCTA images from a single OCT image and took the generated high-quality OCTA images to substitute the original low-quality OCTA images affected by motion artifacts. Li et al. [122] proposed a DL-based motion artifact correction method. This method consists of two networks: the first subnet is applied to detect B-scans affected by eye movement and remove them from the construction of an en-face OCTA image. The second subnet is then designed to reconnect the broken vascular networks in those image regions affected by eye movement. These methods of replacing image patches affected by eye movement with AI-generated ones can generally suppress such motion artifacts; however, the AI-supplemented image information is normally not so complete as the ground truth image is not so easy to generate. Lin et al. [123] utilized adjacent OCTA images for fusion to mitigate motion artifacts, thereby obtaining high-quality OCTA labels. They employed deep learning methods to leverage these high-quality label images for motion artifact-suppressed OCTA image generation from both adjacent and repeated OCT scans. Wang et al. [124] proposed an artificial intelligence–based projection-resolved OCTA method (aiPR-OCTA). In this approach, rule-based signal attenuation-compensated projection-resolved OCTA (sacPR-OCTA) was first employed, where expert graders manually optimized parameters to refine flow signals across different anatomical layers. This process effectively suppresses background noise and artifacts while preserving true flow signals and pathological features, thereby providing high-quality ground truth data for model training. By leveraging a CNN to process both OCT and OCTA data, aiPR-OCTA significantly reduces projection artifacts commonly observed in conventional OCTA. Compared to existing algorithms, aiPR-OCTA not only suppresses projection artifacts but also demonstrates substantial improvements in flow signal-to-noise ratio and background noise reduction. Figure 15 illustrates the results before and after projection artifact removal using aiPR-OCTA, demonstrating the effectiveness of AI-based artifact suppression in OCTA [124]. For signal processing-related artifacts. The accurate segmentation of different retinal layers is crucial in avoiding segmentation error artifacts in OCTA images. Algorithms based on the newest machine vision AI technology have demonstrated satisfactory results for retinal layer segmentation. Researchers, such as Xie et al. [125] and Shah et al. [99] have utilized DL techniques to achieve more precise segmentation results across multiple retinal layers. As the evolution of DL segmentation models continues, researchers can anticipate further improvements in the accuracy and speed of layer segmentation. Regarding doubling artifacts or stretching artifacts, the DL model can be designed to first identify these pattern-specific artifacts and then remove this redundant information through further image processing steps. Furthermore, AI has been utilized in some studies for the assessment of OCTA image quality. For instance, in researches conducted by Dhodapkar et al. [126] and Lauermann et al. [127], DL models were trained to grade quality of OCTA images with various artifacts. These image quality assessments are based on specific image parameters such as motion artifact score, segmentation artifact score, centration on the fovea, and the visual clarity of small capillaries,

whose label values are given by human graders in training. Given the significant influence of OCTA image quality on reliable image analysis, these AI-based image quality grading systems can play a vital role in image interpretation and disease diagnosis. They can also detect the presence of improper operation artifacts, thereby guiding operators to recapture images when necessary.

Table 2. Summary of AI-based methods for OCTA artifact processing.

Authors	Artifact Type and Issues Addressed	Method/Network Structure	Input and Label (Ground Truth)	Function and Advantages
Stefan and Lee (2020) [42]	Projection artifact; Enhancement of low-SNR images; Graph extraction	CNN-based toolbox with enhancement, segmentation, and graphing modules	Input: Raw OCTA images with tail artifact Label: Manually annotated vascular structures	Suppresses tail artifact; Enhances blood flow continuity; Automates multiple stages including enhancement, segmentation, and graph extraction
Mei et al. (2020) [121]	Projection artifact	U-Net	Input: B-scan OCTA (flow signal overlay on structural OCT) with projection artifact Label: Corrected B-scan OCTA (3D-PAR output)	Effectively removes projection artifacts in OCTA data
Guo et al. (2019) [19]	Shadowing artifact; Non-perfusion area identification	Multi-scaled encoder–decoder network (MEDnet-V2)	Input: En-face OCTA images Label: Segmented non-perfusion areas (NPAs) vs. shadow artifacts	Accurately distinguishes NPA from shadow artifacts; Enhances segmentation accuracy
Hossbach et al. (2020) [69]	Motion artifact	DL model for translating structural OCT B-scans to motion-corrected OCTA B-scans	Input: Single B-scan OCT images Label: Corrected B-scan OCTA images	Generates artifact-free OCTA images to replace motion-degraded scans, thereby reducing motion artifacts
Li et al. (2021) [122]	Motion artifact; Artifact detection and vessel reconstruction	Two-stage DL model: ① CLNet for B-scan artifact classification (residual CNN) ② SegNet (dense U-Net) + ComNet (gated encoder–decoder) for vessel structure recovery	CLNet: Input: B-scan OCTA images Label: Clean vs. B-scan OCTA image with motion artifact (manually labeled) SegNet and ComNet: Input: Broken OCTA images with vessel masks Label: Ground truth vessel masks without motion artifact	CLNet accurately detects motion-corrupted B-scans (98.5% accuracy); SegNet + ComNet restores vascular continuity by learning topological features; Robust against various artifact patterns
Lin et al. (2024) [123]	Motion artifact	Fusion of adjacent and repeated B-scans + DL generation model	Input: Repeated and adjacent OCT scans Label: Fused high-quality OCTA images	Leverages multiple scans to generate motion-suppressed OCTA images

Table 2. *Cont.*

Authors	Artifact Type and Issues Addressed	Method/Network Structure	Input and Label (Ground Truth)	Function and Advantages
Wang et al. (2025) [124]	Projection artifact	CNN trained with sacPR-OCTA labels	Input: OCT and OCTA data Label: Expert-optimized sacPR-OCTA images	Effectively reduces projection artifacts, enhances SNR, and preserves clinically relevant pathological features
Shah et al. (2018) [99]	Segmentation error artifact; Precise retinal layer segmentation	CNN based framework for simultaneous multiple surface segmentation	Input: B-scan OCT images Label: Manual annotations of retinal layer boundaries	Performs direct segmentation of each B-scan in a single pass
Xie et al. (2023) [125]	Segmentation error artifact; Precise retinal layer segmentation	U-Net with constrained differentiable dynamic programming (DDP) module	Input: B-scan OCT images Label: Correct retinal layer segmentations	Achieves end-to-end learning for retinal OCT surface segmentation while explicitly enforcing surface smoothness
Dhodapkar et al. (2022) [126]	Comprehensive quality-related artifacts; OCTA image quality assessment	ResNet152	Input: Superficial capillary plexus OCTA images Label: Manual gradings by two independent graders	Achieves high AUCs: 0.99 for low-quality and 0.97 for high-quality image identification
Lauermann et al. (2019) [127]	Comprehensive quality-related artifacts; OCTA image quality assessment	DCNN, DL-based image quality grading	Input: En-face OCTA images Label: Images defined as sufficient or insufficient image quality based on MAS and SAS	Grades artifacts like motion, segmentation, foveal centration; Guides re-acquisition

Currently, most AI-based studies on OCTA artifact processing are still in the experimental development phase, encountering several critical challenges that need to be solved before clinical implementation. A central concern is the scarcity of datasets containing OCTA images and their corresponding counterparts after artifact processing, which restricts the volume of available data for model training and limits model generalization. Furthermore, a significant proportion of studies heavily depend on internal datasets for validation, lacking comprehensive testing on external devices or multi-center clinical data. Furthermore, addressing domain differences among various OCTA devices is imperative for enhancing the robustness of AI performance. On the other hand, current AI artifact processing studies predominantly focus on specific artifact types, while in clinical applications, an ideal scenario entails a holistic approach capable of handling multiple artifact types. Successfully overcoming these challenges will contribute to the practical application and further advancement of AI in OCTA artifact processing. In practical applications, OCTA requires swift and precise artifact suppression to produce immediate and clear images. The ongoing advancement of AI technology offers the promise of real-time artifact suppression, thereby providing invaluable support to clinicians for better visualization and accurate diagnosis. We look forward to further enhancements in AI for artifact processing, ultimately leading to more reliable and efficient clinical evaluations based on OCTA imaging.

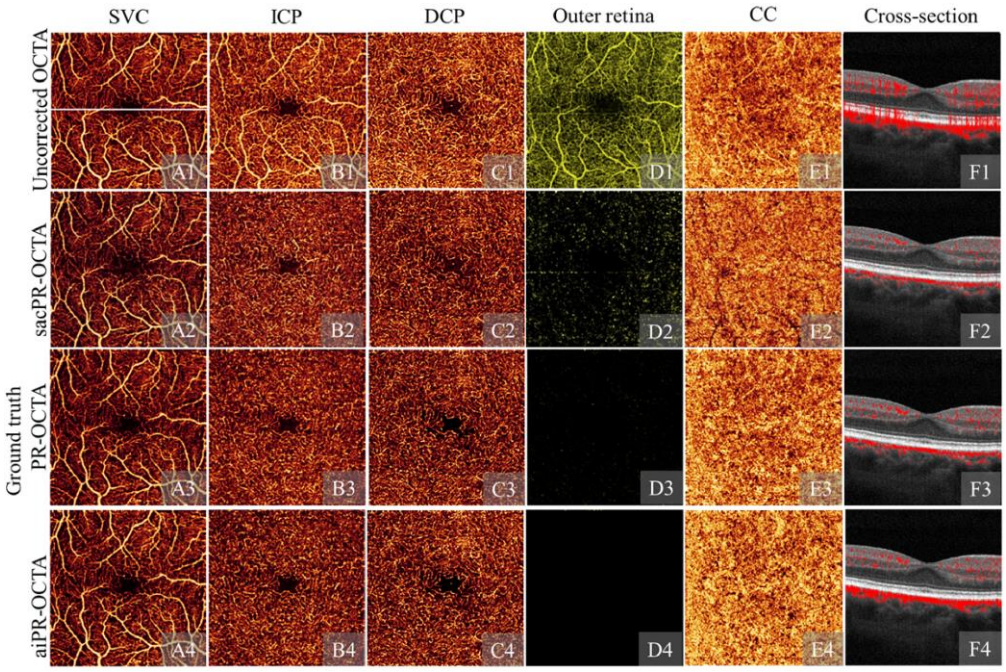


Figure 15. Representative results of AI-based artifact suppression in OCTA. This figure demonstrates the effectiveness of aiPR-OCTA in reducing projection artifacts and preserving vascular detail across retinal and choroidal layers, compared with conventional methods. Row 1: Uncorrected OCTA showing significant projection artifacts in deeper layers. Row 2: sacPR-OCTA with partial artifact suppression but signal attenuation under large vessels. Row 3: Ground truth OCTA manually optimized by expert graders for AI model training. Row 4: aiPR-OCTA showing clean outer retina, uniform choriocapillaris (CC), and preserved microvasculature. Columns A–E: En-face angiograms of SVC, ICP, DCP, outer retina, and CC. Column F: Cross-sectional OCT with red flow overlay, aligned to the white line in A1 [124].

5. Discussion

In general, artifacts in OCTA are prevalent even in normal eye scans [74] and can significantly impact the interpretation of OCTA images when used in clinical diagnosis and monitoring of retinal diseases, as they may be misleading with respect to the true representation of the retinal microvasculature and pathology. However, it is not an easy task to specifically evaluate the impact of OCTA artifacts seen in different OCT devices on clinical practice as it is compounded by quite a number of factors that affect the prevalence and severity of artifacts seen in clinical OCTA images. These factors may include, but not be limited to, scan size (e.g., 3 mm × 3 mm vs. 6 mm × 6 mm) [55], subject (e.g., normal vs. DR or AMD patients) [128], system type (e.g., SD-OCT vs. SS-OCT) [48], device brand (e.g., Zeiss vs. Optovue), which might include different OCTA processing algorithms (e.g., OMAG vs. SSADA) [129], and signal quality (e.g., low vs. high OCT signal) [84,130]. Consequently, some semi-quantitative grading systems were proposed for the effective assessment of artifact severity and its potential influence on retinal disease diagnosis [70,84,131], although these grading systems have not been widely adopted in clinics up to date. It should be also noted that artifacts themselves are, to a certain extent, reflections of tissue pathologies [132] so extreme caution should be exercised for clinicians when interpreting retinal disease conditions considering the potential inaccurate or misleading symptoms caused by artifacts in OCTA images scanned from different patients using specific devices.

OCTA artifacts, if present, could significantly affect the accurate diagnosis of various retinal diseases in clinics. For example, shadowing and defocus artifacts can obscure or distort vascular structures, leading to inaccuracies in measurements such as vessel

density and the foveal avascular zone, which are critical for assessing conditions like DR and AMD. Motion artifacts, most probably resulting from patient eye movements during image acquisition, can cause misalignment and duplication of vascular features, which might obscure critical features like microaneurysms and areas of non-perfusion in DR, potentially leading to underestimation of disease severity. Projection artifacts, although less prevalent, pose a significant challenge by introducing false flow signals in deeper retinal layers, potentially complicating the assessment of the deep capillary plexus, leading to inaccuracies in evaluating capillary dropout and neovascularization in DR. Segmentation errors are particularly problematic in eyes with retinal pathologies, where anatomical disruptions can lead to incorrect layer delineation [133]. Such errors can significantly alter quantitative metrics and hinder accurate disease monitoring. A study of measurement repeatability also shows the intra-class coefficient is lower for the measured vessel density of the deep retinal layer than the superficial layer, most probably because of projection artifacts, necessitating its correction [134].

Artifact correction methods in OCTA have significantly enhanced diagnostic accuracy and measurement repeatability. Various techniques, including hardware-based solutions, algorithmic approaches, and deep learning models [135], have been developed to address common artifacts with solid quantitative data support. Preclinical studies showed that combining real-time eye tracking with motion correction technology (MCT) has proven effective in mitigating motion artifacts. For instance, integrating tracking-assisted scanning with MCT reduced total artifact prevalence by 76% in healthy eyes and 88% in diabetic eyes compared to scans without tracking. This integration also improved the similarity between repeated scans, indicating enhanced repeatability [64]. Quantitative results also clearly showed the advantage of eye motion correction in clinical measurement; for example, Lauermann et al. reported a signal strength index of 53.55 vs. 57.18, a coefficient of variability of vessel density between the first and second measurement of 8.9% vs. 5.7% and a motion artifact score of 3.27 vs. 1.93 at the cost of a slightly longer acquisition time (15.97 s vs. 22.88 s) before and after the use of eye tracking technology in AMD patients [70]. Advanced motion correction algorithms have been developed to further improve image alignment and reduce residual distortions with demonstrated clinical effectiveness. Ploner et al. [59] demonstrated that incorporating OCTA data into motion correction algorithms significantly improved transverse alignment and reduced residual distortion, especially in elderly patients with retinal pathologies. Deussen et al. [136] recently demonstrated that 55% of corrected OCTAs exhibited improved quality after manual layer segmentation correction, leading to a notable increase in the proportion of high-quality images from 63 to 83%. In other studies, it is also quantitatively shown correction of projection artifacts and segmentation errors could help improve the clinical diagnosis and disease treatment monitoring in DR and AMD patients [128,137–139].

In this review, artifacts are categorized into four major types: light propagation-related, motion artifacts, improper operation, and signal processing-related. In our opinion, the difficulty of correcting these artifacts varies based on their origin and the effectiveness of current correction methods. The relative difficulty in correcting these four types of OCTA artifacts can be ranked as motion artifact $\approx$ light propagation-related > signal processing-related > improper operation, based on the following considerations. While real-time eye tracking and post-processing algorithms have been developed to mitigate motion artifacts, complete elimination remains challenging, especially in patients with unstable fixation. Advanced algorithms, such as projection artifact removal techniques, have been implemented to address the correction of projection artifacts, but the complete removal of false flows and accurate extraction of true flows underneath is still a difficult task, particularly in complex cases. In extreme cases of the existence of the first two types of

artifacts, such as complete signal shadowing or constantly unstable fixation, no vasculature or purely noisy signal will be seen in OCTA images, leading to a complete loss of the OCTA's functionality. Therefore, the first two types of OCTA are ranked as the most difficult types for correction. Signal processing-related artifacts such as segmentation errors, although not so easy to correct using algorithms in some complex pathologies, can be fixed through time-consuming manual operation, and therefore are ranked as the intermediate type with respect to the level of correction difficulty. Improper operation-related artifacts are the least difficult to correct as they can be solved by professional training for equipment operation and in situ repeated scanning if needed. It should be noted that although recent fast advancements in projection artifact removal algorithms have mitigated some types of artifacts in OCTA imaging, residual artifacts generally remain, which can still affect image interpretation.

This review provides a description of various types of artifacts that can assist OCTA technicians or clinicians in interpreting OCTA images more accurately and reducing the impact of artifacts on fundus disease diagnosis and evaluation. However, the successful translation of these findings into clinical practice remains a key challenge. Laboratory advances have significantly improved image resolution and diagnostic capabilities, but real-world clinical conditions—such as variability in patient cooperation and disease complexity—pose difficulties not encountered in controlled environments. As OCTA continues to evolve, bridging the gap between laboratory progress and clinical application is critical to maximize its utility in retinal disease diagnosis and management.

6. Future Research Directions and Conclusions

OCTA is a non-invasive, fast, and high-resolution imaging method that can reveal the microvascular network of different retinal layers, offering great potential for clinical applications in diagnosing and treating various retinal diseases. The state of the art in clinical OCTA technology reflects significant advancements, which include higher resolution imaging, wider imaging field of view, larger imaging depth, faster imaging speed, more quantitative analysis algorithms, and integration with other imaging modalities. The enhanced image resolution provides unprecedented clarity for visualizing tissue blood flow. Achieving a larger imaging depth and a wider field of view enables a more comprehensive assessment of the ocular vascular system, extending the application of OCTA to diagnose conditions such as glaucoma, vitreoretinal diseases, choroidal abnormalities, and corneal disorders. The faster imaging speed contributes to less interference from patient motion. Comprehensive blood flow imaging algorithms have been developed to accurately capture intricate microvascular networks. The concurrent development of quantitative analysis algorithms enhances the objective measurement and analysis of blood flow in OCTA images. The integration with other imaging modalities allows for a more comprehensive and complete evaluation of retinal conditions. Notably, the integration of artificial intelligence technology into OCTA analysis facilitates automated image interpretation, aiding in the diagnosis of various conditions, such as diabetic retinopathy and age-related macular degeneration.

With further development of OCTA devices, some OCTA imaging artifacts are expected to be significantly reduced. For example, using faster lasers (swept-source, vertical cavity surface emitting laser, etc.) and increasing the scanning speed will automatically reduce the overall motion artifacts, and reducing overall scanning time with fast OCT systems will also help lower the number of eye movement artifacts in the images. However, a shorter B-scan frame interval will reduce the sensitivity to slow blood flow, and therefore the acquisition speed also needs to be balanced with small blood flow detection [140]. Kolb et al. [141] employed a MHz-OCT system for imaging, utilizing a 1060 nm Fourier

Domain Mode Locked (FDML) laser with a depth scan rate of 1.68 MHz. This high-speed acquisition significantly reduced the presence of motion artifacts. In addition, improving the real-time tracking performance can also reduce motion artifacts, and graphic processing unit (GPU) processing is one of the key factors involved in this process. Consequently, using faster tracking scans with powerful GPUs can suppress more motion artifacts. Algorithm improvement can also reduce the occurrence rate of artifacts. Now, image reconstruction based on artificial intelligence has been proven to be capable of removing some artifacts and improving the signal-to-noise ratio in generating OCTA data from complex signals. Using deep learning can achieve better image reconstruction for specific scenarios, suppress the tailing artifacts of blood vessels, and enable OCTA to achieve realistic 3D vascular structure imaging. Deep learning can also better identify the features of various artifacts and accurately quantify the OCTA data with artifacts [19].

Image artifacts are a major issue in OCTA image interpretation and quantification. Studying the sources and effects of OCTA artifacts is of great significance for clinical diagnosis and evaluation. The research on reducing or eliminating OCTA image artifacts will continue to develop in the future. As the research progresses, more systematic definitions for various types of artifacts will be proposed, and better solutions for their elimination will be developed. It is also meaningful to propose more reasonable and practical artifact grading systems for OCTA images, which will facilitate the assessment of OCTA images [84]. In the future, OCTA technology will continue to develop towards faster scanning speed and larger scanning range, which will enable OCTA imaging to obtain higher resolution and higher quality microvascular images with fewer artifacts. At the same time, further algorithm development will improve the accuracy and repeatability of OCTA quantitative analysis, which will make this technology more widely applied to the diagnosis and treatment evaluation of corresponding retinal diseases. With continuous technological and methodological improvements, OCTA holds great promise for broader and more accurate clinical applications.

Author Contributions: Methodology, Z.L., Y.H. (Yitao Hu) and Y.H. (Yanping Huang); writing—original draft preparation, Z.L., Y.H. (Yitao Hu) and Y.H. (Yanping Huang); writing—review and editing, all authors; visualization, Z.L., Y.H. (Yitao Hu) and Y.H. (Yanping Huang); funding acquisition, G.L., J.X., J.Q., L.A. and Y.H. (Yanping Huang). All authors have read and agreed to the published version of the manuscript.

Funding: This work was funded by the National Natural Science Foundation of China (62001114, 61871130), the Guangdong Provincial Pearl River Talents Program (2019ZT08Y105), the Foshan HKUST Projects (FSUST21-HKUST10E), the Guangdong Eye Intelligent Medical Imaging Equipment Engineering Technology Research Center (2022E076), and the Guangdong-Hong Kong-Macao Intelligent Micro-Nano Optoelectronic Technology Joint Laboratory (2020B1212030010).

Conflicts of Interest: G.L., J.X. and Y.H. (Yanping Huang) are consultants at Weiren Meditech Co., Ltd. J.Q. and L.A. are currently working at Weiren Meditech Co., Ltd. The remaining authors have no disclosure. The funders had no role in the design of the study; in the collection, analyses, or interpretation of data; in the writing of the manuscript; or in the decision to publish the results.

References

1. Huang, D.; Swanson, E.A.; Lin, C.P.; Schuman, J.S.; Stinson, W.G.; Chang, W.; Hee, M.R.; Flotte, T.; Gregory, K.; Puliafito, C.A. Optical coherence tomography. *Science* **1991**, *254*, 1178–1181. [CrossRef] [PubMed]
2. Drexler, W.; Liu, M.; Kumar, A.; Kamali, T.; Unterhuber, A.; Leitgeb, R. Optical coherence tomography today: Speed, contrast, and multimodality. *J. Biomed. Opt.* **2014**, *19*, 071412. [CrossRef]
3. Cogliati, A.; Canavesi, C.; Hayes, A.; Tankam, P.; Duma, V.-F.; Santhanam, A.; Thompson, K.P.; Rolland, J.P. MEMS-based handheld scanning probe with pre-shaped input signals for distortion-free images in Gabor-domain optical coherence microscopy. *Opt. Express* **2016**, *24*, 13365–13374. [CrossRef] [PubMed]

4. Brunner, M.; Romano, V.; Steger, B.; Vinciguerra, R.; Lawman, S.; Williams, B.; Hicks, N.; Czanner, G.; Zheng, Y.; Willoughby, C.E.; et al. Imaging of corneal neovascularization: Optical coherence tomography angiography and fluorescence angiography. *Investig. Ophthalmol. Vis. Sci.* **2018**, *59*, 1263–1269. [CrossRef]
5. Chalam, K.V.; Sambhav, K. Optical coherence tomography angiography in retinal diseases. *J. Ophthal Vis. Res.* **2016**, *11*, 84–92. [CrossRef] [PubMed]
6. Jia, Y.; Bailey, S.T.; Hwang, T.S.; McClintic, S.M.; Gao, S.S.; Pennesi, M.E.; Flaxel, C.J.; Lauer, A.K.; Wilson, D.J.; Hornegger, J.; et al. Quantitative optical coherence tomography angiography of vascular abnormalities in the living human eye. *Proc. Natl. Acad. Sci. USA* **2015**, *112*, E2395–E2402. [CrossRef]
7. Chen, C.L.; Wang, R.K. Optical coherence tomography based angiography. *Biomed. Opt. Express* **2017**, *8*, 1056–1082. [CrossRef]
8. Fingler, J.; Schwartz, D.; Yang, C.; Fraser, S.E. Mobility and transverse flow visualization using phase variance contrast with spectral domain optical coherence tomography. *Opt. Express* **2007**, *15*, 12636–12653. [CrossRef]
9. Kim, D.Y.; Fingler, J.; Werner, J.S.; Schwartz, D.M.; Fraser, S.E.; Zawadzki, R.J. In vivo volumetric imaging of human retinal circulation with phase-variance optical coherence tomography. *Biomed. Opt. Express* **2011**, *2*, 1504–1513. [CrossRef]
10. Mariampillai, A.; Standish, B.A.; Moriyama, E.H.; Khurana, M.; Munce, N.R.; Leung, M.K.; Jiang, J.; Cable, A.; Wilson, B.C.; Vitkin, I.A.; et al. Speckle variance detection of microvasculature using swept-source optical coherence tomography. *Opt. Lett.* **2008**, *33*, 1530–1532. [CrossRef]
11. Blatter, C.; Klein, T.; Grajciar, B.; Schmoll, T.; Wieser, W.; Andre, R.; Huber, R.; Leitgeb, R.A. Ultrahigh-speed non-invasive widefield angiography. *J. Biomed. Opt.* **2012**, *17*, 070505. [CrossRef]
12. Wang, R.K.; Jacques, S.L.; Ma, Z.; Hurst, S.; Hanson, S.R.; Gruber, A. Three dimensional optical angiography. *Opt. Express* **2007**, *15*, 4083–4097. [CrossRef] [PubMed]
13. Wang, R.K.; An, L.; Saunders, S.; Wilson, D.J. Optical microangiography provides depth-resolved images of directional ocular blood perfusion in posterior eye segment. *J. Biomed. Opt.* **2010**, *15*, 020502. [CrossRef] [PubMed]
14. Wang, R.K. Optical microangiography: A label-free 3-D imaging technology to visualize and quantify blood circulations within tissue beds in vivo. *IEEE J. Sel. Top. Quantum Electron.* **2010**, *16*, 545–554. [CrossRef]
15. Stanga, P.E.; Lim, J.I.; Hamilton, P. Indocyanine green angiography in chorioretinal diseases: Indications and interpretation-An evidence-based update. *Ophthalmology* **2003**, *110*, 15–21. [CrossRef]
16. Hope-Ross, M.; Yannuzzi, L.A.; Gragoudas, E.S.; Guyer, D.R.; Slakter, J.S.; Sorenson, J.A.; Krupsky, S.; Orlock, D.A.; Puliafito, C.A. Adverse reactions due to indocyanine green. *Ophthalmology* **1994**, *101*, 529–533. [CrossRef] [PubMed]
17. Lopez-Saez, M.P.; Ordoqui, E.; Tornero, P.; Baeza, A.; Sainza, T.; Zubeldia, J.M.; Baeza, M.L. Fluorescein-induced allergic reaction. *Ann. Allergy Asthma Immunol.* **1998**, *81*, 428–430. [CrossRef]
18. Hagag, A.M.; Gao, S.S.; Jia, Y.; Huang, D. Optical coherence tomography angiography: Technical principles and clinical applications in ophthalmology. *Taiwan. J. Ophthalmol.* **2017**, *7*, 115–129. [CrossRef]
19. Guo, Y.; Hormel, T.T.; Xiong, H.; Wang, B.; Camino, A.; Wang, J.; Huang, D.; Hwang, T.S.; Jia, Y. Development and validation of a deep learning algorithm for distinguishing the nonperfusion area from signal reduction artifacts on OCT angiography. *Biomed. Opt. Express* **2019**, *10*, 3257–3268. [CrossRef]
20. Parodi, M.B.; Cicinelli, M.V.; Rabiolo, A.; Pierro, L.; Gagliardi, M.; Bolognesi, G.; Bandello, F. Vessel density analysis in patients with retinitis pigmentosa by means of optical coherence tomography angiography. *Br. J. Ophthalmol.* **2017**, *101*, 428–432. [CrossRef]
21. Chidambara, L.; Gadde, S.G.K.; Yadav, N.K.; Jayadev, C.; Bhanushali, D.; Appaji, A.M.; Akkali, M.; Khurana, A.; Shetty, R. Characteristics and quantification of vascular changes in macular telangiectasia type 2 on optical coherence tomography angiography. *Br. J. Ophthalmol.* **2016**, *100*, 1482–1488. [CrossRef] [PubMed]
22. Iftikhar, M.; Zafar, S.; Gonzalez, N.; Murphy, O.; Kwakyi, M.S.O.; Feldman, B.S.S.; Calabresi, P.A.; Saidha, S.; Channa, R. Image artifacts in optical coherence tomography angiography among patients with multiple sclerosis. *Curr. Eye Res.* **2019**, *44*, 558–563. [CrossRef] [PubMed]
23. Arya, M.; Rashad, R.; Sorour, O.; Moult, E.M.; Fujimoto, J.G.; Waheed, N.K. Optical coherence tomography angiography (OCTA) flow speed mapping technology for retinal diseases. *Expert. Rev. Med. Devices* **2018**, *15*, 875–882. [CrossRef]
24. Hormel, T.T.; Huang, D.; Jia, Y. Artifacts and artifact removal in optical coherence tomographic angiography. *Quant. Imaging Med. Surg.* **2021**, *11*, 1120–1133. [CrossRef]
25. Barton, J.K.; Stromski, S. Flow measurement without phase information in optical coherence tomography images. *Opt. Express* **2005**, *13*, 5234–5239. [CrossRef]
26. Jia, Y.; Tan, O.; Tokayer, J.; Potsaid, B.; Wang, Y.; Liu, J.J.; Kraus, M.F.; Subhash, H.; Fujimoto, J.G.; Hornegger, J.; et al. Split-spectrum amplitude-decorrelation angiography with optical coherence tomography. *Opt. Express* **2012**, *20*, 4710–4725. [CrossRef]
27. Bazvand, F.; Ghassemi, F. Artifacts in macular optical coherence tomography. *J. Curr. Ophthalmol.* **2020**, *32*, 123–131. [CrossRef]
28. Huang, Y.; Zhang, Q.; Wang, R.K. Efficient method to suppress artifacts caused by tissue hyper-reflections in optical microangiography of retina in vivo. *Biomed. Opt. Express* **2015**, *6*, 1195–1208. [CrossRef] [PubMed]

29. Liu, L.; Gao, S.S.; Bailey, S.T.; Huang, D.; Li, D.; Jia, Y. Automated choroidal neovascularization detection algorithm for optical coherence tomography angiography. *Biomed. Opt. Express* **2015**, *6*, 3564–3576. [CrossRef]
30. Liu, Y.; Carass, A.; Filippatou, A.; He, Y.; Solomon, S.D.; Saidha, S.; Calabresi, P.A.; Prince, J.L. Projection artifact suppression for inner retina in OCT angiography. In Proceedings of the 2019 IEEE 16th International Symposium on Biomedical Imaging (ISBI 2019), Venice, Italy, 8–11 April 2019; pp. 592–596.
31. Wang, J.; Hormel, T.T.; Bailey, S.T.; Hwang, T.S.; Huang, D.; Jia, Y. Signal attenuation-compensated projection-resolved OCT angiography. *Biomed. Opt. Express* **2023**, *14*, 2040–2054. [CrossRef]
32. Wang, R.K. Signal degradation by multiple scattering in optical coherence tomography of dense tissue: A Monte Carlo study towards optical clearing of biotissues. *Phys. Med. Biol.* **2002**, *47*, 2281. [CrossRef] [PubMed]
33. Bhavsar, K.V.; Jia, Y.; Wang, J.; Patel, R.C.; Lauer, A.K.; Huang, D.; Bailey, S.T. Projection-resolved optical coherence tomography angiography exhibiting early flow prior to clinically observed retinal angiomatous proliferation. *Am. J. Ophthalmol. Case Rep.* **2017**, *8*, 53–57. [CrossRef]
34. Leahy, C.; Radhakrishnan, H.; Bernucci, M.; Srinivasan, V.J. Imaging and graphing of cortical vasculature using dynamically focused optical coherence microscopy angiography. *J. Biomed. Opt.* **2016**, *21*, 020502. [CrossRef] [PubMed]
35. Zhang, A.; Zhang, Q.; Wang, R.K. Minimizing projection artifacts for accurate presentation of choroidal neovascularization in OCT micro-angiography. *Biomed. Opt. Express* **2015**, *6*, 4130–4143. [CrossRef]
36. Zhang, M.; Hwang, T.S.; Campbell, J.P.; Bailey, S.T.; Wilson, D.J.; Huang, D.; Jia, Y. Projection-resolved optical coherence tomographic angiography. *Biomed. Opt. Express* **2016**, *7*, 816–828. [CrossRef]
37. Wang, J.; Zhang, M.; Hwang, T.S.; Bailey, S.T.; Huang, D.; Wilson, D.J.; Jia, Y. Reflectance-based projection-resolved optical coherence tomography angiography. *Biomed. Opt. Express* **2017**, *8*, 1536–1548. [CrossRef] [PubMed]
38. Yousefi, S.; Liu, T.; Wang, R.K. Segmentation and quantification of blood vessels for OCT-based micro-angiograms using hybrid shape/intensity compounding. *Microvasc. Res.* **2015**, *97*, 37–46. [CrossRef]
39. Li, P.; Huang, Z.; Yang, S.; Liu, X.; Ren, Q.; Li, P. Adaptive classifier allows enhanced flow contrast in OCT angiography using a histogram-based motion threshold and 3D Hessian analysis-based shape filtering. *Opt. Lett.* **2017**, *42*, 4816–4819. [CrossRef]
40. Tang, J.; Erdener, S.E.; Sunil, S.; Boas, D.A. Normalized field autocorrelation function-based optical coherence tomography three-dimensional angiography. *J. Biomed. Opt.* **2019**, *24*, 036005. [CrossRef]
41. Zhou, J.; Li, Y.; Tang, J. Adaptive dynamic analysis-based optical coherence tomography angiography for blood vessel projection artifact suppression. *Biomed. Opt. Express* **2023**, *14*, 477–488. [CrossRef]
42. Stefan, S.; Lee, J. Deep learning toolbox for automated enhancement, segmentation, and graphing of cortical optical coherence tomography microangiograms. *Biomed. Opt. Express* **2020**, *11*, 7325–7342. [CrossRef] [PubMed]
43. Lang, G.E.; Enders, C.; Loidl, M.; Lang, G.K.; Werner, J.U. Accurate OCT-angiography interpretation-detection and exclusion of artifacts. *Klin. Monatsblatter Augenheilkd.* **2017**, *234*, 1109–1118. [CrossRef]
44. Camino, A.; Jia, Y.; Yu, J.; Wang, J.; Liu, L.; Huang, D. Automated detection of shadow artifacts in optical coherence tomography angiography. *Biomed. Opt. Express* **2019**, *10*, 1514–1531. [CrossRef] [PubMed]
45. Hormel, T.T.; Hwang, T.S.; Bailey, S.T.; Wilson, D.J.; Huang, D.; Jia, Y. Artificial intelligence in OCT angiography. *Prog. Retin. Eye Res.* **2021**, *85*, 100965. [CrossRef]
46. Wei, X.; Hormel, T.T.; Guo, Y.; Hwang, T.S.; Jia, Y. High-resolution wide-field OCT angiography with a self-navigation method to correct microsaccades and blinks. *Biomed. Opt. Express* **2020**, *11*, 3234–3245. [CrossRef]
47. Spaide, R.F.; Fujimoto, J.G.; Waheed, N.K.; Sadda, S.R.; Staurenghi, G. Optical coherence tomography angiography. *Prog. Retin. Eye Res.* **2018**, *64*, 1–55. [CrossRef]
48. Reich, M.; Boehringer, D.; Rothaus, K.; Cakir, B.; Bucher, F.; Daniel, M.; Lang, S.J.; Lagreze, W.A.; Agostini, H.; Lange, C. Swept-source optical coherence tomography angiography alleviates shadowing artifacts caused by subretinal fluid. *Int. Ophthalmol.* **2020**, *40*, 2007–2016. [CrossRef]
49. Hormel, T.T.; Jia, Y.; Jian, Y.; Hwang, T.S.; Bailey, S.T.; Pennesi, M.E.; Wilson, D.J.; Morrison, J.C.; Huang, D. Plexus-specific retinal vascular anatomy and pathologies as seen by projection-resolved optical coherence tomographic angiography. *Prog. Retin. Eye Res.* **2021**, *80*, 100878. [CrossRef]
50. Wei, X.; Hormel, T.T.; Guo, Y.; Jia, Y. 75-degree non-mydriatic single-volume optical coherence tomographic angiography. *Biomed. Opt. Express* **2019**, *10*, 6286–6295. [CrossRef]
51. De Pretto, L.R.; Moult, E.M.; Alibhai, A.Y.; Carrasco-Zevallos, O.M.; Chen, S.; Lee, B.; Witkin, A.J.; Baumal, C.R.; Reichel, E.; de Freitas, A.Z.; et al. Controlling for artifacts in widefield optical coherence tomography angiography measurements of non-perfusion area. *Sci. Rep.* **2019**, *9*, 9096. [CrossRef]
52. Yu, J.J.; Camino, A.; Liu, L.; Zhang, X.; Wang, J.; Gao, S.S.; Jia, Y.; Huang, D. Signal strength reduction effects in OCT angiography. *Ophthalmol. Retin.* **2019**, *3*, 835–842. [CrossRef] [PubMed]

53. Gao, S.S.; Jia, Y.; Liu, L.; Zhang, M.; Takusagawa, H.L.; Morrison, J.C.; Huang, D. Compensation for reflectance variation in vessel density quantification by optical coherence tomography angiography. *Investig. Ophthalmol. Vis. Sci.* **2016**, *57*, 4485–4492. [CrossRef] [PubMed]
54. Chlebiej, M.; Gorczynska, I.; Rutkowski, A.; Kluczewski, J.; Grzona, T.; Pijewska, E.; Sikorski, B.L.; Szkulmowska, A.; Szkulmowski, M. Quality improvement of OCT angiograms with elliptical directional filtering. *Biomed. Opt. Express* **2019**, *10*, 1013–1031. [CrossRef] [PubMed]
55. Cui, Y.; Zhu, Y.; Wang, J.C.; Lu, Y.; Zeng, R.; Katz, R.; Wu, D.M.; Vavvas, D.G.; Husain, D.; Miller, J.W.; et al. Imaging artifacts and segmentation errors with wide-field swept-source optical coherence tomography angiography in diabetic retinopathy. *Transl. Vis. Sci. Technol.* **2019**, *8*, 18. [CrossRef] [PubMed]
56. Falavarjani, K.G.; Al-Sheikh, M.; Akil, H.; Sadda, S.R. Image artefacts in swept-source optical coherence tomography angiography. *Br. J. Ophthalmol.* **2017**, *101*, 564–568. [CrossRef]
57. Wang, Y.; Bo, Q.; Jia, H.; Sun, M.; Yu, Y.; Huang, P.; Wang, J.; Xu, N.; Wang, F.; Wang, H.; et al. Small dome-shaped pigment epithelium detachment in polypoidal choroidal vasculopathy: An under-recognized sign of polypoidal lesions on optical coherence tomography? *Eye* **2021**, *36*, 733–741. [CrossRef]
58. Kraus, M.F.; Potsaid, B.; Mayer, M.A.; Bock, R.; Baumann, B.; Liu, J.J.; Hornegger, J.; Fujimoto, J.G. Motion correction in optical coherence tomography volumes on a per A-scan basis using orthogonal scan patterns. *Biomed. Opt. Express* **2012**, *3*, 1182–1199. [CrossRef]
59. Ploner, S.B.; Kraus, M.F.; Moult, E.M.; Husvogt, L.; Schottenhamml, J.; Alibhai, A.Y.; Waheed, N.K.; Duker, J.S.; Fujimoto, J.G.; Maier, A.K. Efficient and high accuracy 3-D OCT angiography motion correction in pathology. *Biomed. Opt. Express* **2021**, *12*, 125–146. [CrossRef]
60. Zang, P.; Liu, G.; Zhang, M.; Dongye, C.; Wang, J.; Pechauer, A.D.; Hwang, T.S.; Wilson, D.J.; Huang, D.; Li, D. Automated motion correction using parallel-strip registration for wide-field en face OCT angiogram. *Biomed. Opt. Express* **2016**, *7*, 2823–2836. [CrossRef]
61. Spaide, R.F.; Fujimoto, J.G.; Waheed, N.K. Image artifacts in optical coherence tomography angiography. *Retina* **2015**, *35*, 2163–2180. [CrossRef]
62. Vienola, K.V.; Braaf, B.; Sheehy, C.K.; Yang, Q.; Tiruveedhula, P.; Arathorn, D.W.; de Boer, J.F.; Roorda, A. Real-time eye motion compensation for OCT imaging with tracking SLO. *Biomed. Opt. Express* **2012**, *3*, 2950–2963. [CrossRef] [PubMed]
63. Zhang, Q.; Huang, Y.; Zhang, T.; Kubach, S.; An, L.; Laron, M.; Sharma, U.; Wang, R.K. Wide-field imaging of retinal vasculature using optical coherence tomography-based microangiography provided by motion tracking. *J. Biomed. Opt.* **2015**, *20*, 066008. [CrossRef] [PubMed]
64. Camino, A.; Zhang, M.; Gao, S.S.; Hwang, T.S.; Sharma, U.; Wilson, D.J.; Huang, D.; Jia, Y. Evaluation of artifact reduction in optical coherence tomography angiography with real-time tracking and motion correction technology. *Biomed. Opt. Express* **2016**, *7*, 3905–3915. [CrossRef]
65. Camino, A.; Zhang, M.; Dongye, C.; Pechauer, A.D.; Hwang, T.S.; Bailey, S.T.; Lujan, B.; Wilson, D.J.; Huang, D.; Jia, Y. Automated registration and enhanced processing of clinical optical coherence tomography angiography. *Quant. Imaging Med. Surg.* **2016**, *6*, 391–401. [CrossRef]
66. Zang, P.; Liu, G.; Zhang, M.; Wang, J.; Hwang, T.S.; Wilson, D.J.; Huang, D.; Li, D.; Jia, Y. Automated three-dimensional registration and volume rebuilding for wide-field angiographic and structural optical coherence tomography. *J. Biomed. Opt.* **2017**, *22*, 026001. [CrossRef] [PubMed]
67. Kraus, M.F.; Liu, J.J.; Schottenhamml, J.; Chen, C.-L.; Budai, A.; Branchini, L.; Ko, T.; Ishikawa, H.; Wollstein, G.; Schuman, J.; et al. Quantitative 3D-OCT motion correction with tilt and illumination correction, robust similarity measure and regularization. *Biomed. Opt. Express* **2014**, *5*, 2591–2613. [CrossRef]
68. Camino, A.; Jia, Y.; Liu, G.; Wang, J.; Huang, D. Regression-based algorithm for bulk motion subtraction in optical coherence tomography angiography. *Biomed. Opt. Express* **2017**, *8*, 3053–3066. [CrossRef]
69. Hossbach, J.; Husvogt, L.; Kraus, M.F.; Fujimoto, J.G.; Maier, A.K. Deep OCT angiography image generation for motion artifact suppression. In *Bildverarbeitung für die Medizin 2020*; Springer: Wiesbaden, Germany, 2020; pp. 248–253.
70. Lauermann, J.L.; Treder, M.; Heiduschka, P.; Clemens, C.R.; Eter, N.; Alten, F. Impact of eye-tracking technology on OCT-angiography imaging quality in age-related macular degeneration. *Graef Arch. Clin. Exp.* **2017**, *255*, 1535–1542. [CrossRef]
71. Cheng, W.; Song, Y.; Lin, F.; Xiong, J.; Li, F.; Jin, L.; Wang, Z.; Yang, C.; Yang, B.; Wang, F.; et al. Assessment of artifacts in swept-source optical coherence tomography angiography for glaucomatous and bormal eyes. *Transl. Vis. Sci. Technol.* **2022**, *11*, 23. [CrossRef]
72. Enders, C.; Lang, G.E.; Dreyhaupt, J.; Loidl, M.; Lang, G.K.; Werner, J.U. Quantity and quality of image artifacts in optical coherence tomography angiography. *PLoS ONE* **2019**, *14*, e0210505. [CrossRef]

73. Murphy, O.C.; Kwakyi, O.; Iftikhar, M.; Zafar, S.; Lambe, J.; Pellegrini, N.; Sotirchos, E.S.; Gonzalez-Caldito, N.; Ogbuokiri, E.; Filippatou, A.; et al. Alterations in the retinal vasculature occur in multiple sclerosis and exhibit novel correlations with disability and visual function measures. *Ophthalmol. Retin.* **2020**, *26*, 815–828. [CrossRef]
74. Abu-Yaghi, N.E.; Obiedat, A.F.; AlNawaiseh, T.I.; Hamad, A.M.; Ata, B.A.B.; Quzli, A.A.; AlRyalat, S.A. Optical coherence tomography angiography in healthy adult subjects: Bormative values, frequency, and impact of artifacts. *Biomed. Res. Int.* **2022**, *2022*, 7286252. [CrossRef] [PubMed]
75. Chen, F.K.; Viljoen, R.D.; Bukowska, D.M. Classification of image artefacts in optical coherence tomography angiography of the choroid in macular diseases. *Clin. Exp. Ophthalmol.* **2016**, *44*, 388–399. [CrossRef]
76. Walther, J.; Mueller, G.; Morawietz, H.; Koch, E. Signal power decrease due to fringe washout as an extension of the limited Doppler flow measurement range in spectral domain optical coherence tomography. *J. Biomed. Opt.* **2010**, *15*, 041511. [CrossRef]
77. Brown, T.G.; Cogswell, C.J.; Wilson, T.; Meemon, P.; Palawong, K.; Pongchalee, P. Simplified methods of design, implementation, and characterization of a spectrometer-based FD-OCT. In Proceedings of the Three-Dimensional and Multidimensional Microscopy: Image Acquisition and Processing XXI, San Francisco, CA, USA, 3–6 February 2014; pp. 232–237.
78. Yun, S.; Tearney, G.; De Boer, J.; Bouma, B. Motion artifacts in optical coherence tomography with frequency-domain ranging. *Opt. Express* **2004**, *12*, 2977–2998. [CrossRef] [PubMed]
79. Hua, R.; Wang, H. Dark signals in the choroidal vasculature on optical coherence tomography angiography: An artefact or not? *J. Ophthalmol.* **2017**, *2017*, 5498125. [CrossRef] [PubMed]
80. Kamalipour, A.; Moghimi, S.; Hou, H.; Penteado, R.C.; Hyuk, W.; Proudfoot, J.A.; El-Nimri, N.; Ekici, E.; Rezapour, J.; Zangwill, L.M.; et al. OCT angiography artifacts in glaucoma. *Ophthalmology* **2021**, *128*, 1426–1437. [CrossRef]
81. Chhablani, J.; Krishnan, T.; Sethi, V.; Kozak, I. Artifacts in optical coherence tomography. *Saudi J. Ophthalmol.* **2014**, *28*, 81–87. [CrossRef]
82. Czako, C.; Istvan, L.; Benyo, F.; Elo, A.; Erdei, G.; Horvath, H.; Nagy, Z.Z.; Kovacs, I. The impact of deterministic signal loss on OCT angiography measurements. *Transl. Vis. Sci. Technol.* **2020**, *9*, 10. [CrossRef]
83. Raevis, J.; Etheridge, T.; Cleland, S.; Mititelu, M. Autoimmune retinopathy: Findings and limitations from optical coherence tomography angiography. *Int. J. Retin. Vitr.* **2020**, *6*, 64. [CrossRef]
84. Holmen, I.C.; Konda, S.M.; Pak, J.W.; McDaniel, K.W.; Blodi, B.; Stepien, K.E.; Domalpally, A. Prevalence and severity of artifacts in optical coherence tomographic angiograms. *JAMA Ophthalmol.* **2020**, *138*, 119–126. [CrossRef]
85. Kim, M.; Zhou, X.; Wuppukondur, S.N.; Jiang, X.; Wang, R.K.; Kashani, A.H. Characterizing and quantifying image artifacts in optical coherence tomography angiograms of normal retinal vasculature. *Investig. Ophthalmol. Vis. Sci.* **2022**, *63*, 2939–F0092.
86. Pierro, L.; Aragona, E.; Arrigo, A.; Gagliardi, M.; Bandello, F. The mirror artifact effect on OCTA reconstructions of patients with high myopia. *Spektrum Augenheilkd.* **2017**, *31*, 257–261. [CrossRef]
87. Falavarjani, K.G.; Khadamy, J.; Safi, H.; Karimi, N.; Amirkourjani, F. Effect of grid decentration on macular thickness measurements in normal subjects and patients with diabetic macular edema. *Eur. J. Ophthalmol.* **2015**, *25*, 218–221. [CrossRef]
88. Li, M.C.; Chen, Y.R.; Ji, Z.X.; Xie, K.R.; Yuan, S.T.; Chen, Q.; Li, S. Image projection network: 3D to 2D image segmentation in OCTA images. *IEEE Trans. Med. Imaging* **2020**, *39*, 3343–3354. [CrossRef] [PubMed]
89. Ho, J.; Sull, A.C.; Vuong, L.N.; Chen, Y.; Liu, J.; Fujimoto, J.G.; Schuman, J.S.; Duker, J.S. Assessment of artifacts and reproducibility across spectral- and time-domain optical coherence tomography devices. *Ophthalmology* **2009**, *116*, 1960–1970. [CrossRef] [PubMed]
90. Lentzsch, A.; Schoellhorn, L.; Schnorr, C.; Siggel, R.; Liakopoulos, S. Comparison of swept-source versus spectral-domain optical coherence tomography angiography for detection of macular neovascularization. *Graef Arch. Clin. Exp.* **2022**, *260*, 113–119. [CrossRef]
91. Han, I.C.; Jaffe, G.J. Evaluation of artifacts associated with macular spectral-domain optical coherence tomography. *Ophthalmology* **2010**, *117*, 1177–1189.e1174. [CrossRef]
92. Spaide, R.F.; Curcio, C.A. Evaluation of segmentation of the superficial and deep vascular layers of the retina by optical coherence tomography angiography instruments in normal eyes. *JAMA Ophthalmol.* **2017**, *135*, 259–262. [CrossRef]
93. Hwang, Y.H.; Kim, M.K.; Kim, D.W. Segmentation errors in macular ganglion cell analysis as determined by optical coherence tomography. *Ophthalmology* **2016**, *123*, 950–958. [CrossRef]
94. Domalpally, A.; Danis, R.P.; Zhang, B.; Myers, D.; Kruse, C.N. Quality issues in interpretation of optical coherence tomograms in macular diseases. *Retina* **2009**, *29*, 775–781. [CrossRef] [PubMed]
95. Fabritius, T.; Makita, S.; Miura, M.; Myllyla, R.; Yasuno, Y. Automated segmentation of the macula by optical coherence tomography. *Opt. Express* **2009**, *17*, 15659–15669. [CrossRef]
96. Ahlers, C.; Simader, C.; Geitzenauer, W.; Stock, G.; Stetson, P.; Dastmalchi, S.; Schmidt-Erfurth, U. Automatic segmentation in three-dimensional analysis of fibrovascular pigmentepithelial detachment using high-definition optical coherence tomography. *Br. J. Ophthalmol.* **2008**, *92*, 197–203. [CrossRef]

97. Pekala, M.; Joshi, N.; Liu, T.Y.A.; Bressler, N.M.; DeBuc, D.C.; Burlina, P. Deep learning based retinal OCT segmentation. *Comput. Biol. Med.* **2019**, *114*, 103445. [CrossRef] [PubMed]
98. Li, Q.; Li, S.; He, Z.; Guan, H.; Chen, R.; Xu, Y.; Wang, T.; Qi, S.; Mei, J.; Wang, W. DeepRetina: Layer Segmentation of Retina in OCT Images Using Deep Learning. *Transl. Vis. Sci. Technol.* **2020**, *9*, 61. [CrossRef]
99. Shah, A.; Zhou, L.; Abramoff, M.D.; Wu, X. Multiple surface segmentation using convolution neural nets: Application to retinal layer segmentation in OCT images. *Biomed. Opt. Express* **2018**, *9*, 4509–4526. [CrossRef] [PubMed]
100. Chiu, S.J.; Li, X.T.; Nicholas, P.; Toth, C.A.; Izatt, J.A.; Farsiu, S. Automatic segmentation of seven retinal layers in SDOCT images congruent with expert manual segmentation. *Opt. Express* **2010**, *18*, 19413–19428. [CrossRef]
101. Zang, P.; Gao, S.S.; Hwang, T.S.; Flaxel, C.J.; Wilson, D.J.; Morrison, J.C.; Huang, D.; Li, D.; Jia, Y. Automated boundary detection of the optic disc and layer segmentation of the peripapillary retina in volumetric structural and angiographic optical coherence tomography. *Biomed. Opt. Express* **2017**, *8*, 1306–1318. [CrossRef]
102. Zhang, M.; Wang, J.; Pechauer, A.D.; Hwang, T.S.; Gao, S.S.; Liu, L.; Liu, L.; Bailey, S.T.; Wilson, D.J.; Huang, D.; et al. Advanced image processing for optical coherence tomographic angiography of macular diseases. *Biomed. Opt. Express* **2015**, *6*, 4661–4675. [CrossRef]
103. Kugelman, J.; Alonso-Caneiro, D.; Read, S.A.; Vincent, S.J.; Collins, M.J. Automatic segmentation of OCT retinal boundaries using recurrent neural networks and graph search. *Biomed. Opt. Express* **2018**, *9*, 5759–5777. [CrossRef]
104. Guo, Y.; Camino, A.; Zhang, M.; Wang, J.; Huang, D.; Hwang, T.; Jia, Y. Automated segmentation of retinal layer boundaries and capillary plexuses in wide-field optical coherence tomographic angiography. *Biomed. Opt. Express* **2018**, *9*, 4429–4442. [CrossRef] [PubMed]
105. Zang, P.; Wang, J.; Hormel, T.T.; Liu, L.; Huang, D.; Jia, Y. Automated segmentation of peripapillary retinal boundaries in OCT combining a convolutional neural network and a multi-weights graph search. *Biomed. Opt. Express* **2019**, *10*, 4340–4352. [CrossRef]
106. Sui, X.; Zheng, Y.; Wei, B.; Bi, H.; Wu, J.; Pan, X.; Yin, Y.; Zhang, S. Choroid segmentation from optical coherence tomography with graph edge weights learned from deep convolutional neural networks. *Neurocomputing* **2017**, *237*, 332–341. [CrossRef]
107. de Sisternes, L.; Jonna, G.; Moss, J.; Marmor, M.F.; Leng, T.; Rubin, D.L. Automated intraretinal segmentation of SD-OCT images in normal and age-related macular degeneration eyes. *Biomed. Opt. Express* **2017**, *8*, 1926–1949. [CrossRef]
108. Treder, M.; Lauermann, J.L.; Eter, N. Automated detection of exudative age-related macular degeneration in spectral domain optical coherence tomography using deep learning. *Graef Arch. Clin. Exp.* **2018**, *256*, 259–265. [CrossRef]
109. Bogunovic, H.; Waldstein, S.M.; Schlegl, T.; Langs, G.; Sadeghipour, A.; Liu, X.; Gerendas, B.S.; Osborne, A.; Schmidt-Erfurth, U. Prediction of anti-VEGF treatment requirements in neovascular AMD using a machine learning approach. *Investig. Ophthalmol. Vis. Sci.* **2017**, *58*, 3240–3248. [CrossRef] [PubMed]
110. Pohlmann, D.; Berlin, M.; Reidl, F.; Kuenzel, S.E.; Pleyer, U.; Joussen, A.M.; Winterhalter, S. Longitudinal comparison of constant artifacts in optical coherence tomography angiography in patients with posterior uveitis compared to healthy subjects. *J. Clin. Med.* **2022**, *11*, 5376. [CrossRef] [PubMed]
111. Eastline, M.; Munk, M.R.; Wolf, S.; Schaal, K.B.; Ebneter, A.; Tian, M.; Giannakaki-Zimmermann, H.; Zinkernagel, M.S. Repeatability of wide-field optical coherence tomography angiography in normal retina. *Transl. Vis. Sci. Technol.* **2019**, *8*, 6. [CrossRef]
112. Ho, J.; Dans, K.; You, Q.; Nudleman, E.N.; Freeman, W.R. Comparison of 3 × 3 mm versus 6 × 6 mm optical coherence tomography angiography scan sizes in the evaluation of non-proliferative diabetic retinopathy. *Retina* **2019**, *39*, 259–264. [CrossRef]
113. Bontzos, G.; Kabanarou, S.A.; Garnavou-Xirou, C.; Gkizis, I.; Kontou, E.; Triantafyllou, D.; Xirou, T. Segmentation errors and motion artifacts in OCTA associated with epiretinal membranes. *Can. J. Ophthalmol.* **2020**, *55*, 293–300. [CrossRef]
114. Tan, A.C.; Tan, G.S.; Denniston, A.K.; Keane, P.A.; Ang, M.; Milea, D.; Chakravarthy, U.; Cheung, C.M.G. An overview of the clinical applications of optical coherence tomography angiography. *Eye* **2018**, *32*, 262–286. [CrossRef] [PubMed]
115. Yang, D.; Ran, A.R.; Nguyen, T.X.X.; Lin, T.P.H.; Chen, H.; Lai, T.Y.Y.; Tham, C.C.C.; Cheung, C.Y.Y. Deep learning in optical coherence tomography angiography: Current progress, challenges, and future directions. *Diagnostics* **2023**, *13*, 326. [CrossRef] [PubMed]
116. Yoo, T.K.; Choi, J.Y.; Kim, H.K. Feasibility study to improve deep learning in OCT diagnosis of rare retinal diseases with few-shot classification. *Med. Biol. Eng. Comput.* **2021**, *59*, 401–415. [CrossRef] [PubMed]
117. Yang, D.; Tang, Z.; Ran, A.; Nguyen, T.X.; Szeto, S.; Chan, J.; Wong, C.Y.; Hui, V.; Tsang, K.; Chan, C.K. Assessment of parafoveal diabetic macular ischemia on optical coherence tomography angiography images to predict diabetic retinal disease progression and visual acuity deterioration. *JAMA Ophthalmol.* **2023**, *141*, 641–649. [CrossRef]
118. Jia, H.; Lu, B.; Zhao, Z.; Yu, Y.; Wang, F.; Zhou, M.; Sun, X. Prediction of the short-term efficacy of anti-VEGF therapy for neovascular age-related macular degeneration using optical coherence tomography angiography. *Eye Vis.* **2022**, *9*, 16. [CrossRef]
119. Alryalat, S.A.; Al-Antary, M.; Arafa, Y.; Azad, B.; Boldyreff, C.; Ghnaimat, T.; Al-Antary, N.; Alfegi, S.; Elfalah, M.; Abu-Ameerh, M. Deep learning prediction of response to anti-VEGF among diabetic macular edema patients: Treatment response analyzer system (TRAS). *Diagnostics* **2022**, *12*, 312. [CrossRef]

120. Kashani, A.H.; Liu, T.A.; Jones, C. Optical Coherence Tomography Angiography, Artificial Intelligence, and the Missing Capillaries. *JAMA Ophthalmol.* **2023**, *141*, 649–650. [CrossRef]
121. Mei, S.; Mao, Z.; Wang, Z.; Chan, K. Deep-learning-based projection artifact removal in optical coherence tomography angiography volumes. *Investig. Ophthalmol. Vis. Sci.* **2020**, *61*, 4577.
122. Li, A.; Du, C.; Pan, Y. Deep-learning-based motion correction in optical coherence tomography angiography. *J. Biophotonics* **2021**, *14*, e202100097. [CrossRef]
123. Lin, Z.; Zhang, Q.; Lan, G.; Xu, J.; Qin, J.; An, L.; Huang, Y. Deep learning for motion artifact-suppressed OCTA image generation from both repeated and adjacent OCT scans. *Mathematics* **2024**, *12*, 446. [CrossRef]
124. Wang, J.; Hormel, T.T.; Bailey, S.T.; Hwang, T.S.; Jia, Y. Artificial intelligence-assisted projection-resolved optical coherence tomographic angiography (aiPR-OCTA). *Opt. Express* **2025**, *33*, 16658–16670. [CrossRef]
125. Xie, H.; Xu, W.; Xing, Y.X.; Wu, X. Deep learning network with differentiable dynamic programming for retina OCT surface segmentation. *Biomed. Opt. Express* **2023**, *14*, 3190–3202. [CrossRef]
126. Dhodapkar, R.M.; Li, E.; Nwanyanwu, K.; Adelman, R.; Krishnaswamy, S.; Wang, J.C. Deep learning for quality assessment of optical coherence tomography angiography images. *Sci. Rep.* **2022**, *12*, 13775. [CrossRef] [PubMed]
127. Lauermann, J.L.; Treder, M.; Alnawaiseh, M.; Clemens, C.R.; Eter, N.; Alten, F. Automated OCT angiography image quality assessment using a deep learning algorithm. *Graef Arch. Clin. Exp.* **2019**, *257*, 1641–1648. [CrossRef]
128. Falavarjani, K.G.; Habibi, A.; Anvari, P.; Ghasemizadeh, S.; Khorasani, M.A.; Shenazandi, H.; Sarraf, D. Effect of segmentation error correction on optical coherence tomography angiography measurements in healthy subjects and diabetic macular oedema. *Br. J. Ophthalmol.* **2020**, *104*, 162–166. [CrossRef]
129. Li, X.-X.; Wu, W.; Zhou, H.; Deng, J.-J.; Zhao, M.-Y.; Qian, T.-W.; Yan, C.; Xu, X.; Yu, S.-Q. A quantitative comparison of five optical coherence tomography angiography systems in clinical performance. *Int. J. Ophthalmol.* **2018**, *11*, 1784–1795. [CrossRef] [PubMed]
130. Ali, N.; Sampson, D.M.; Yong, A.A.; Jeewa, R.; Rajgopal, S.; Dutt, D.D.C.S.; Mohamed, S.; Mohamed, S.; Menghini, M.; Hansen, A.; et al. Clinical validation of the RTVue optical coherence tomography angiography image quality indicators. *Clin. Exp. Ophthalmol.* **2020**, *48*, 192–203. [CrossRef]
131. Lauermann, J.L.; Woetzel, A.K.; Treder, M.; Alnawaiseh, M.; Clemens, C.R.; Eter, N.; Alten, F. Prevalences of segmentation errors and motion artifacts in OCT-angiography differ among retinal diseases. *Graef Arch. Clin. Exp.* **2018**, *256*, 1807–1816. [CrossRef]
132. Scuderi, L.; Fragiotta, S.; Ciancimino, C.; Mafrici, M.; Mazzola, M.; Varano, M.; Rossi, T.; Parravano, M. Leveraging optical coherence tomography and angiography artifacts to identify clinicopathological correlates in macular disorders. *Photonics* **2024**, *11*, 991. [CrossRef]
133. Greig, E.C.; Duker, J.S.; Waheed, N.K. A practical guide to optical coherence tomography angiography interpretation. *Int. J. Retin. Vitr.* **2020**, *6*, 55. [CrossRef]
134. Al-Sheikh, M.; Ghasemi Falavarjani, K.; Akil, H.; Sadda, S.R. Impact of image quality on OCT angiography based quantitative measurements. *Int. J. Retin. Vitr.* **2017**, *3*, 13. [CrossRef] [PubMed]
135. Chen, K.; Yang, X.; Na, J.; Wang, W. Denoising, segmentation and volumetric rendering of optical coherence tomography angiography (OCTA) image using deep learning techniques: A review. *arXiv* **2025**, arXiv:2502.14935.
136. Deussen, D.N.; Heinke, A.; Elsner, W.; Galang, C.M.B.; Kalaw, F.G.P.; Warter, A.; Bartsch, D.-U.; Cheng, L.; Freeman, W.R. Effect of manual OCTA segmentation correction to improve image quality and visibility of choroidal neovascularization in AMD. *Sci. Rep.* **2024**, *14*, 13990. [CrossRef] [PubMed]
137. Binotti, W.W.; Romano, A.C. Investigative ophthalmology visual science. *Investig. Ophthalmol. Vis. Sci.* **2019**, *60*, 1321–1327. [CrossRef] [PubMed]
138. Zhang, Q.; Zhang, A.; Lee, C.S.; Lee, A.Y.; Rezaei, K.A.; Roisman, L.; Miller, A.; Zheng, F.; Gregori, G.; Durbin, M.K.; et al. Projection artifact removal improves visualization and quantitation of macular neovascularization imaged by optical coherence tomography angiography. *Ophthalmol. Retin.* **2017**, *1*, 124–136. [CrossRef]
139. Ghasemi Falavarjani, K.; Mirshahi, R.; Ghasemizadeh, S.; Sardarinia, M. Stepwise segmentation error correction in optical coherence tomography angiography images of patients with diabetic macular edema. *Ther. Adv. Ophthalmol.* **2020**, *12*, 2515841420947931. [CrossRef]
140. Cheng, Y.; Guo, L.; Pan, C.; Lu, T.; Hong, T.; Ding, Z.; Li, P. Statistical analysis of motion contrast in optical coherence tomography angiography. *J. Biomed. Opt.* **2015**, *20*, 116004. [CrossRef]
141. Kolb, J.P.; Klein, T.; Kufner, C.L.; Wieser, W.; Neubauer, A.S.; Huber, R. Ultra-widefield retinal MHz-OCT imaging with up to 100 degrees viewing angle. *Biomed. Opt. Express* **2015**, *6*, 1534–1552. [CrossRef]

Disclaimer/Publisher's Note: The statements, opinions and data contained in all publications are solely those of the individual author(s) and contributor(s) and not of MDPI and/or the editor(s). MDPI and/or the editor(s) disclaim responsibility for any injury to people or property resulting from any ideas, methods, instructions or products referred to in the content.